



Design and analysis of a new wave energy converter based on a point absorber and a hydraulic system harvesting energy from waves near the shore in calm seas

Silvio Barbarelli  | Mario Amelio | Teresa Castiglione  | Gaetano Florio | Nino Michele Scornaienchi

Department of Mechanical, Energy and Management Engineering, University of Calabria, Rende, Italy

Correspondence

Silvio Barbarelli, Department of Mechanical, Energy and Management Engineering, University of Calabria, Ponte Bucci, Cubo 44C, Rende 87036, Italy.
Email: silvio.barbarelli@unical.it

Summary

The aim of this paper is to illustrate the design of a new wave energy converter, composed of a point absorber and a hydraulic system (power take off) and sized for recovering energy in calm seas from waves near the shore. The point absorber is consisting of a rectangular shaped buoy integrating a piston pump. The set buoy-pump oscillates under the waves action and moves natural water in a closed circuit hydraulic system (power take off) composed of a piping connecting the piston pump itself, a pressurized reservoir, a hydraulic turbine and a discharge tank. The methodology adopted for designing the main constituents involves a 1D mathematical model, settled for understanding the motion of the buoy under the hypothesis of regular waves and fully developed sea, and a sizing procedure applied for the design of all the components of the hydraulic system. The project related to the Calabrian site of Cetraro (Mediterranean Sea—south Italy) led to designing a system with a 4 m large buoy, associated with a small 13 cm diameter micro Pelton turbine, so that more than 22 000 kWh could be recovered in a year.

KEYWORDS

energy output estimation, Pelton turbine, piston pump, point absorber, pressure control, sizing procedure, wave energy, WEC

1 | INTRODUCTION

In an energy scenario, even more troubled by the exhaustion of fossil fuels, renewable energies coming from sea offer a substantial contribution to their replacement.¹ The exploitation of the wave potential has been estimated to grow considerably in the next few decades, promoting the spread of Wave Energy Converters (WEC).² Moreover, renewable energy storage technologies will play an important role in the management of the energy supply.³

At present, several WECs have been developed and tested⁴; however, no installation has obtained a massive commercial success.⁵

Wave energy converter systems combined with a floating breakwater can be seen as a cost-effective solution and at the same time provide a coastal protection. This will make wave energy competitive and will start production of commercial-scale wave power converters.⁶

Floating offshore wind platform combined with Wave Energy Converters (WECs) systems have instead the possibility to provide a cost-effective solution to offshore power supply and platform protection.⁷

In countries surrounded by sea and oceans or in island, where the wave potential is very high, research on wave energy production is particularly dynamic. In Europe, the countries situated along the Atlantic Coast

such as, Portugal, Spain, Ireland, Norway, and the UK are the most interested in the research and development of WEC.⁸ In islands, the implementation of WECs in micro-grids applications could resolve many problems related to energy supply.

The energy amount extractable from waves is an important factor for the feasibility of a power plant, which over the years should produce more than the installation costs, and so determining the choice of high-potential sites, but often that implies harsh waves which happen during extreme events.

These circumstances raise technical issues affecting the design and arrangement of WECs, sometime raising the costs so much as to make it no longer convenient.⁹ In the Mediterranean Sea, the possibility of working with moderate waves simplifies the design of production plants, making them attractive. Anyway, technical problems related to extreme sea climate could be solved by improving the research, so that wave energy production could be economically viable even in those cases.

However, with the aim to evaluate the feasibility of a wave energy plant, a detailed knowledge of the amount of available energy and its temporal and spatial variability is required.¹⁰

The wave status of the sea is very variable and it is determined by the factors that transfer energy to the wave like winds, seismic disturbances, and lunar and solar gravitational fields. Moreover, the seabed bathymetry or generic obstacles affect the shape and the extension of the waves.

Various idealized spectra have been proposed in oceanography and naval engineering,¹¹ the simplest assumes the waves balanced with the wind and the period of the wave proportional to the square root of the wave height (fully developed sea, Pierson-Moskowitz spectrum¹²). Therefore, the average power, transported by a wave per meter wave front, can be calculated as proportional to the square of the wave height and to the period of the same¹³:

Based on existing similar arrangements,¹⁴ a new wave energy converter (WEC) is here studied and simulated. The main novelty of this work concerns the design of a new kind of point absorber, different from those developed to the present, conceived for exploiting waves near the shore, with crest line almost parallel to the coast and particularly suitable for those sites characterized by a moderate energy flux. The related power take off instead consists of a traditional hydraulic system able to store energy pressure and deliver that to a micro Pelton turbine. The point absorber is integrated with the chamber of a volumetric pump, which moves up and down sliding on a fixed piston. The buoy-pump set oscillates under the waves action moving natural water in a closed piping circuit which in turn connects two tanks: a pressurized

reservoir, feeding the hydraulic micro Pelton turbine and a second tank for the discharge of the turbine.

The authors, differently from others like Bonovas,⁹ Tampier,¹⁵ Shadman,²¹ and Hansen,²⁹ face the calculus of the buoy oscillations both with a traditional differential equations approach and with a simplified method. The latter allows obtaining simplified formulas which correlate the stroke of the piston pump to the height of the waves. These formulas become a useful tool for the performance assessment, giving results affected by errors in the order of 5%. Moreover, they allow all the component of the system to be easily sized and its optimal working condition to be found.

Therefore, with the aim to guarantee optimal performance, pressure and flow rate of the water supplying the turbine are changed¹⁶ as the height of the wave changes.

The objective of this paper is to illustrate an overall-flexible procedure in order to design all the components of the system: the point absorber, the piping, the hydraulic system, and the micro Pelton Turbine. This methodology, supported by a numerical model developed in Matlab-Simulink@ environment, allows a quick sizing in relation of the energy wave potential to be obtained. That is an important finding useful to allow a rapid estimate by the designers for the feasibility of the plant, starting from the energy resource of the site.

To better illustrate that, a case study regarding a plant installation in the Calabrian site of Cetraro (Italy), characterized by a low energy potential, is proposed. The results show that, by implementing small size components with consequent limited costs, it is possible to exploit acceptable quantities of energy in a year.

2 | SYSTEM DESCRIPTION

The system is developed with the aim to convert the wave motion in the vertical motion of a large buoy, successively transformed in pressure energy and finally in electrical energy.

Figure 1A,B gives a schematic of its main components. The absorption point (power take off) can be positioned near the shore, if the seabed allows it and in proximity of breakwaters. In the latter case, two goals could be achieved simultaneously: extension of the shore up to deep waters and reduction of the installations costs, because of the possibility to lay the machinery on the breakwaters. The absorption point is composed of a buoy having a rectangular shape, which incorporates the cylindrical chamber of a piston pump. Under the waves action, the buoy slides on four rods planted in a concrete base and connected among them on the top, while the chamber moves by sliding around the piston, which is

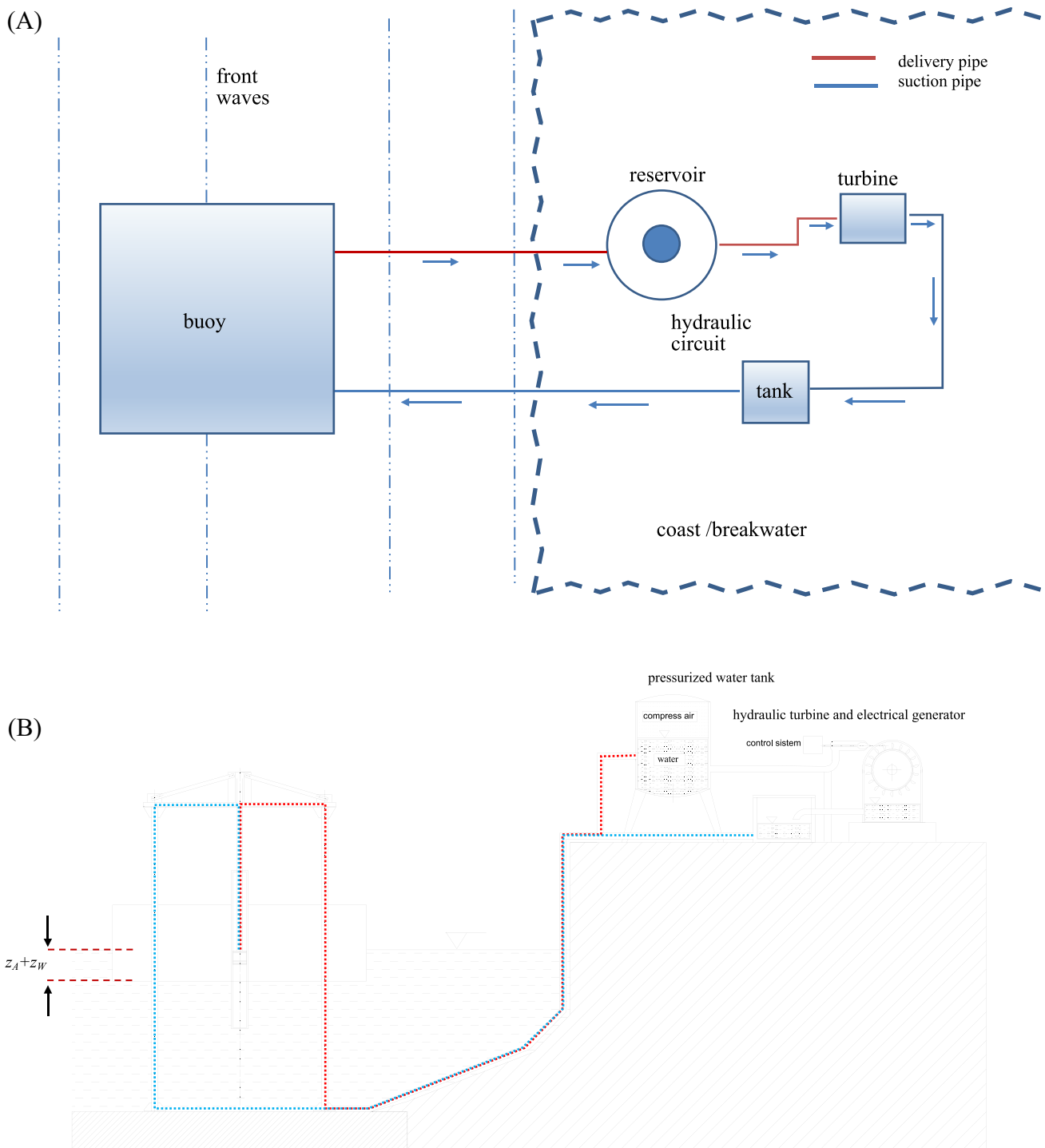


FIGURE 1 System layout. A, Top view and B, side view [Colour figure can be viewed at wileyonlinelibrary.com]

instead fixed. Therefore, an unusual piston pump, having fixed and mobile parts inverted, is realized able to move water in a hydraulic closed circuit. In particular, the fixed piston is pierced and is equipped with two pipes marked in blue and red in Figure 2, through which it pushes and sucks water, as highlighted in Figures 1A,B and 2.

The delivery pipe, marked in red, pushes water into a pressurized reservoir filled partially by air. Because of the solubility of the air in water, an auxiliary compressor can replenish the air losses. Pressurized water feeds a Pelton turbine, which, in turn, drives an electric generator. The discarded water is collected in a tank at atmospheric

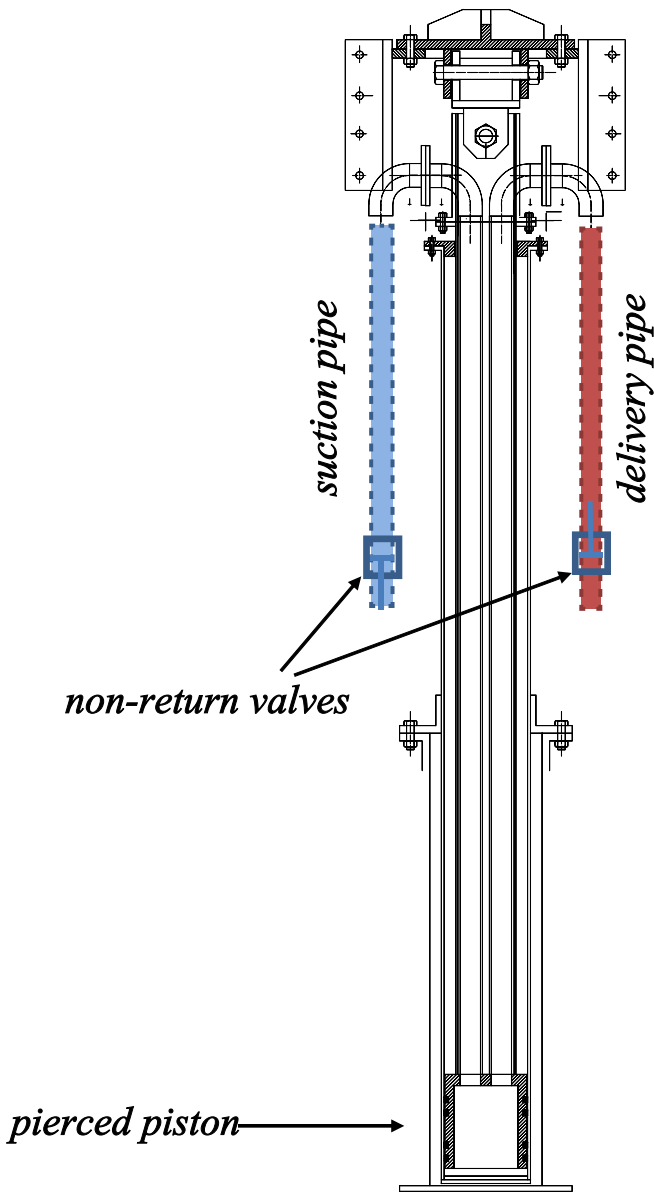


FIGURE 2 Fixed piston particular [Colour figure can be viewed at wileyonlinelibrary.com]

pressure to be sucked out by the pump through the suction pipe, marked in blue.

2.1 | Interaction wave-buoy

The buoy is free to oscillate in the vertical direction (Figure 1B) by following the crests and the troughs of the wave; its oscillating motion allows the pump to push and suck water in the hydraulic circuit. This mechanism is well depicted in Figure 3, which shows how the piston pump moves the water in the hydraulic circuit; the dashed line represents the sea level over time.

When the level of the wave is at its minimum (Figure 3A), the cylinder chamber is completely filled by

water: as the level rises (Figure 3B) the pump chamber reduces its volume by delivering water through the delivery (red) pipe, visible in Figures 1A,B and 2, at the pressurized reservoir. This is the compression phase, which is characterized by the opening of the nonreturn valve in the delivery pipe and the closure of the nonreturn valve in the suction pipe. That occurs until the wave reaches the peak level (Figure 3C). Subsequently, the buoy is dragged down by the wave (Figure 3D,E) by sucking water through the blue pipe (Figures 1A,B and 2) from the atmospheric tank until it reaches again the minimum position (Figure 3F). This is the filling phase, which is characterized by the opening of the nonreturn valve in the suction pipe and the closure of the nonreturn valve in the delivery pipe.

3 | METHODOLOGY

The methodology, applied to the technical analysis of the proposed system, is based on the development of a one-dimensional mathematical model, which determines the buoy vertical oscillation over time. The model has then supported a first sizing of the system, which takes into account geometrical ratios, performance charts, and wave characteristics.

3.1 | Mathematical model

The buoy motion equation is obtained in the time domain with reference to the vertical position, z , of the immersed (bottom) surface of the buoy, which, at still sea ($z = 0$), equals its draft, $-D$ (initial conditions).

In order to simplify the model, a regular wave is assumed. For an oscillating point absorber WEC in a regular wave, with height H_w and circular frequency ω , the radiation force is reduced to a linear damping; moreover, an added mass term is included.¹⁵ By taking into account the exiting wave force, the force exerted by the power take off (PTO), inertia, and friction in the pipes, drag, and radiation damping of the buoy, the motion equation is:

$$\left[m_{buoy} + m_{add} + \rho L_{pipe} A_{pipe} \left(\frac{D_p}{D_{pipe}} \right)^2 \right] \ddot{z} + b \dot{z} + \left[\frac{1}{2} \rho C_D S_w + \frac{1}{2} \rho f A_p \frac{L_{pipe}}{D_{pipe}} \left(\frac{D_p}{D_{pipe}} \right)^2 \right] |\dot{z}| \dot{z} + \rho g A_{buoy} z = F_{ex} - F_{PTO} \quad (1)$$

The forces acting on the buoy are shown in Figure 4. The exciting wave force F_{ex} is given by the hydrodynamic pressure multiplied for the buoy area. For finite water depth, having average water depth h and for a buoy

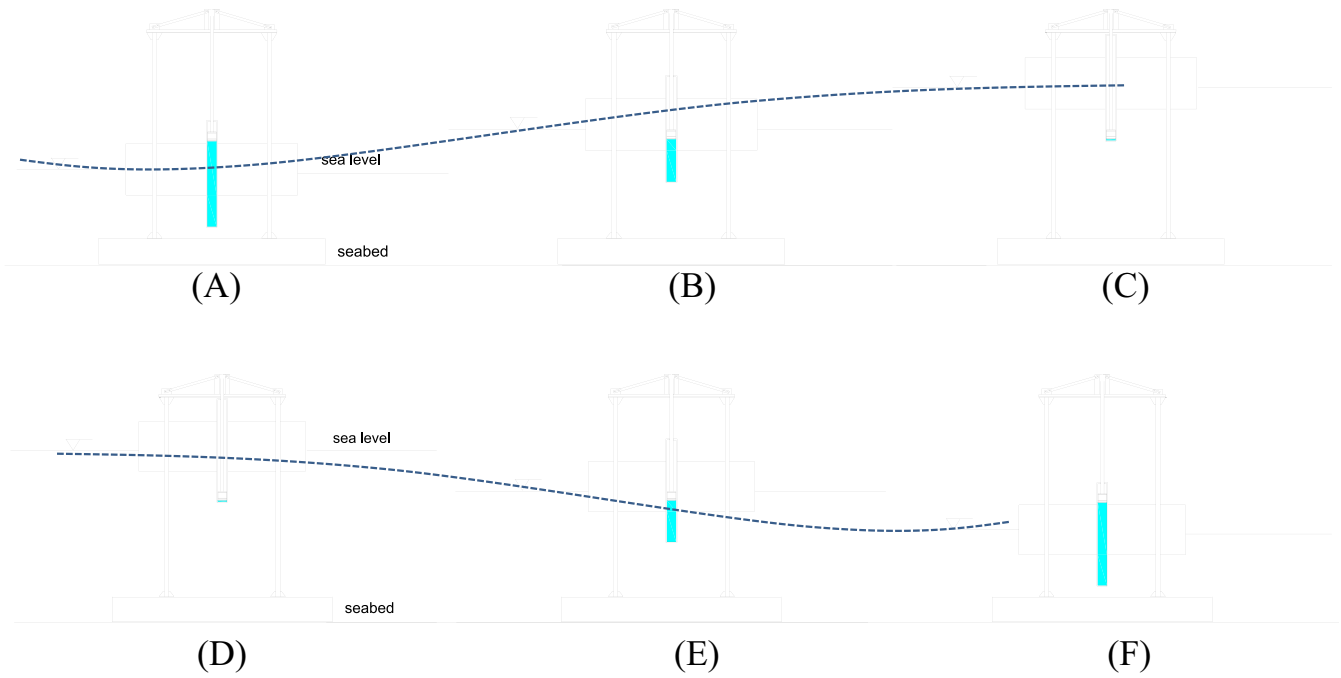


FIGURE 3 Operating cycle of the piston pump [Colour figure can be viewed at wileyonlinelibrary.com]

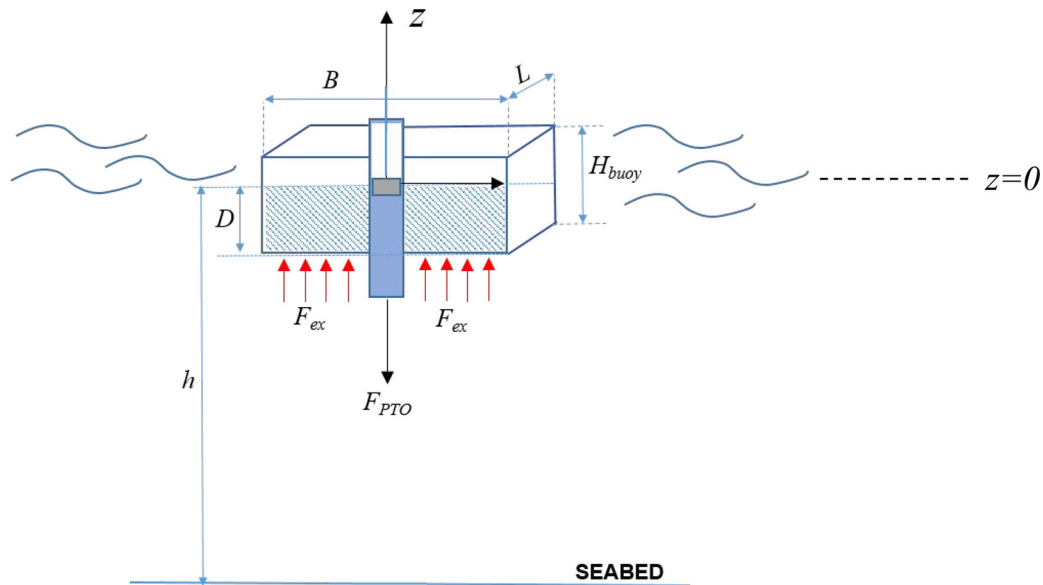


FIGURE 4 Scheme of the forces on the buoy [Colour figure can be viewed at wileyonlinelibrary.com]

characterized by a length L along the wave direction, a width B along the wave front, a height H_{buoy} , and a draft D , it can be expressed as¹⁷:

$$F_{ex} = F_{ex.a} \sin(\omega t) \tag{3}$$

where k , the wave number, for finite water depth is defined as¹⁷:

$$F_{ex} = \rho g \frac{H_w \cosh k(D+h)}{2 \sinh kh} B \int_{-L/2}^{L/2} \sin(\omega t - kx) dx$$

$$= \rho g \frac{H_w \cosh k(D+h)}{2 \sinh kh} \frac{2}{kL} \sin\left(\frac{kL}{2}\right) A_{buoy} \sin(\omega t) \tag{2}$$

$$k \tanh(kh) = \frac{\omega^2}{g} \tag{4}$$

If the buoy is rising and the pump chamber is full of water having a pressure slightly higher than that of the

reservoir, because of the pressure losses along the pipe-line, the power take off force is equal to (see Figure 5):

$$F_{PTO} = F_p + F_W \tag{5}$$

The components of the power take off forces are listed below:

- F_p is the pressure force exerted on the piston pump, which, by taking into account the pressure of the reservoir $p_{res} = \rho g H_m$ (H_m represents the water column meters), the efficiency of the hydraulic piping η_p and the diameter of the piston pump D_p can be computed as:

$$F_p = \frac{\pi D_p^2 \rho g H_m}{4 \eta_p} \tag{6}$$

- F_W is the weight force given by:

$$F_W = g m_{buoy} \tag{7}$$

In this case (buoy rising), being the terms constant, the draft of the buoy D is given by $z_A + z_W$, where z_A is caused by the pressure force (F_p) and z_W is caused by the weight force (F_W)—see Equation (8).

$$z_A = \frac{F_p}{\rho g A_{buoy}} \quad z_W = \frac{F_W}{\rho g A_{buoy}} \tag{8}$$

On the contrary, if the buoy is sinking and the pump chamber is disconnected from the reservoir because of

the nonreturn valve closure (see Figure 2), the power take off force is given by:

$$F_{PTO} = F_W \tag{9}$$

With the downward movement, the chamber of the pump integrated in the buoy increases its volume and draws water from the tank shown in Figure 1A,B (the nonreturn valve opens in the suction pipe—Figure 2). In this case, the sinking of the buoy is simply z_W (see Figure 5).

About the first member of Equation (1), the added mass, m_{add} , and the damping coefficient, b , depend on the circular frequency, ω , on water depth ratio, h/D , and on buoy wetted body shape beam-draft ratio B/D .

Figure 6A,B reports the dimensionless added mass and the dimensionless damping, respectively, as function of the dimensionless circular frequency for three representative different values of the water depth ratio h/D and of the buoy wetted body shape beam-draft ratio B/D . These trends are related to a buoy having a rectangular prism shape, as found in Reference 18.

Equation (1) has to take into account two main phases in a complete buoy oscillation: the rising of the buoy and the falling of the buoy. Moreover, different working conditions must be considered: regular operation and particular cases.

Under regular operation, the buoy is partially immersed in the water ($H_w - H_{buoy} < z < H_w$). During the rising phase, Equation (1), by marking the terms with the subscript 1, can be written as follows:

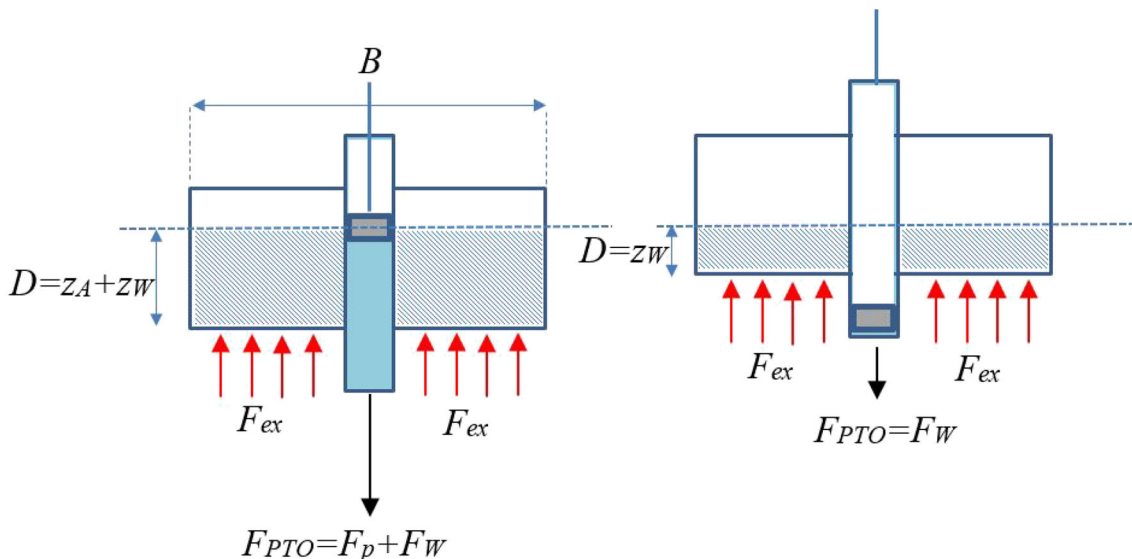


FIGURE 5 Forces on the buoy. Left: buoy rises; Right: buoy sinks [Colour figure can be viewed at wileyonlinelibrary.com]

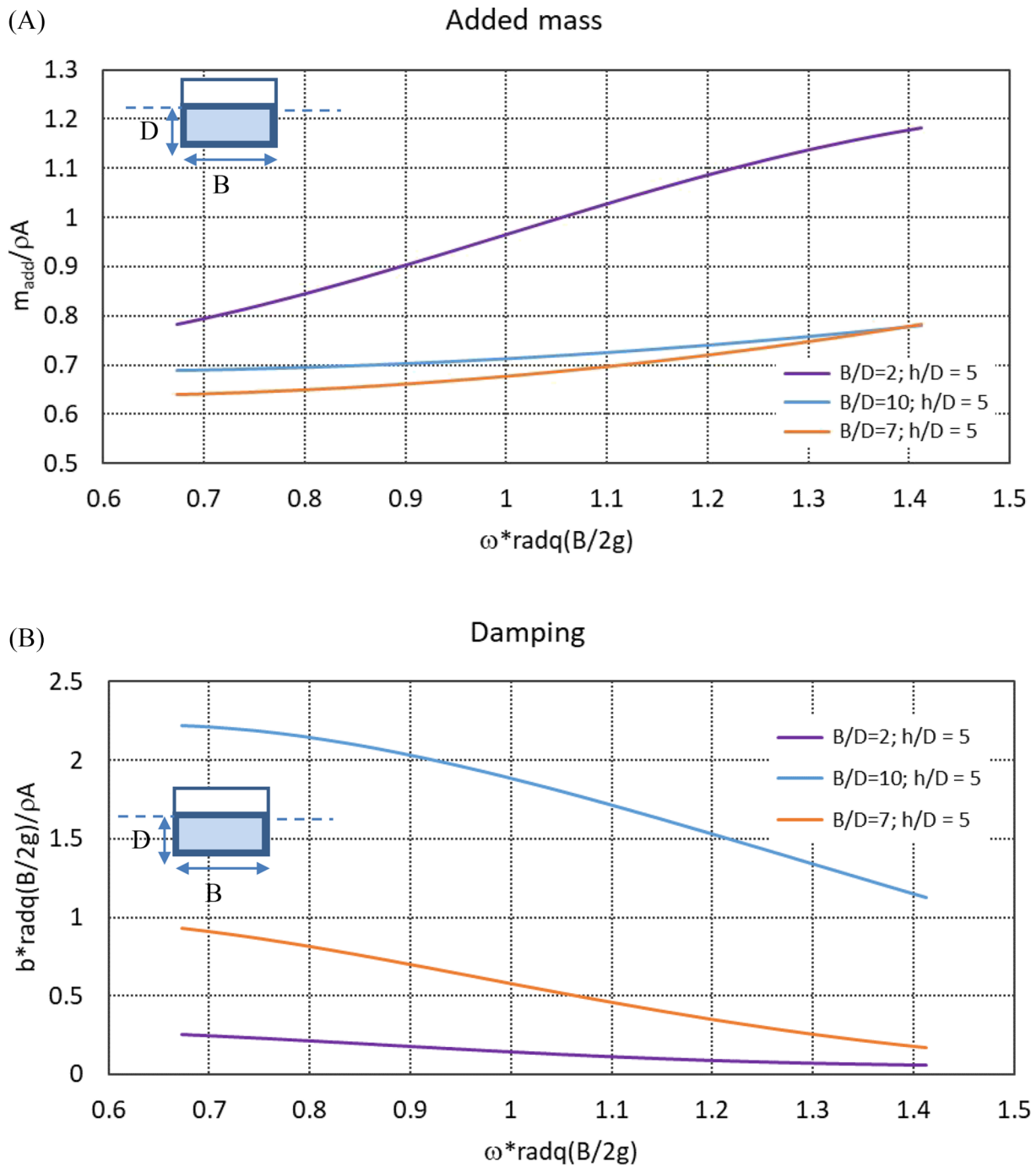


FIGURE 6 A, Dimensionless added mass vs dimensionless circular frequency. B, Dimensionless damping vs dimensionless circular frequency [Colour figure can be viewed at wileyonlinelibrary.com]

$$\begin{aligned}
 & \left[m_{buoy} + m_{add1} + \rho L_{pipe1} A_{pipe1} \left(\frac{D_p}{D_{pipe1}} \right)^2 \right] \ddot{z} + b_1 \dot{z} \\
 & + \left[\frac{1}{2} \rho C_{D1} S_w + \frac{1}{2} \rho f A_p \frac{L_{pipe1}}{D_{pipe1}} \left(\frac{D_p}{D_{pipe1}} \right)^2 \right] |\dot{z}| \dot{z} \\
 & + \rho g A_{buoy} z = \rho g \frac{H_w \cosh k(z_A + z_W + h)}{2 \sinh kh} \frac{2}{kL} \\
 & \times \sin \left(\frac{kL}{2} \right) A_{buoy} \sin(\omega t) - F_p - F_W \tag{10}
 \end{aligned}$$

In this case, the acting forces are the pressure force F_p and the weight force F_W , which determine the draft $D = z_A + z_W$, while m_{add1} and b_1 are valuable by considering a constant draft and by referring to the graphs of Figure 6A,B.

During the falling phase, Equation (1), by marking the terms with the subscript 2, takes the following form:

$$\begin{aligned}
& \left[m_{buoy} + m_{add2} + \rho L_{pipe2} A_{pipe2} \left(\frac{D_p}{D_{pipe2}} \right)^2 \right] \ddot{z} + b_2 \dot{z} \\
& + \left[\frac{1}{2} \rho C_{D2} S_w + \frac{1}{2} \rho f A_p \frac{L_{pipe2}}{D_{pipe2}} \left(\frac{D_p}{D_{pipe2}} \right)^2 \right] |\dot{z}| \dot{z} \\
& + \rho g A_{buoy} z = \rho g \frac{H_w \cosh k(z_w + h)}{2 \sinh kh} \frac{2}{kL} \\
& \times \sin \left(\frac{kL}{2} \right) A_{buoy} \sin(\omega t) - F_W
\end{aligned} \quad (11)$$

In this case, the weight force acts and m_{add2} and b_2 are evaluable by considering the draft $D = z_w$ and by referring to the graphs of Figure 6A,B.

Particular cases occur when the buoy comes up out of water ($z > H_w$) and when the buoy is completely immersed in water ($z < H_w - H_{buoy}$). In the first case, during the rising phase, the equation of motion is given by:

$$\begin{aligned}
& \left[m_{buoy} + \rho L_{pipe1} A_{pipe1} \left(\frac{D_p}{D_{pipe1}} \right)^2 \right] \ddot{z} \\
& + \left[\frac{1}{2} \rho f A_p \frac{L_{pipe1}}{D_{pipe1}} \left(\frac{D_p}{D_{pipe1}} \right)^2 \right] |\dot{z}| \dot{z} = -F_p - F_W
\end{aligned} \quad (12)$$

The acting forces are the pressure force F_p and the weight force F_W , but no action of the waves occurs. During the falling phase, only the weight force acts and the right term of the equation becomes $-F_W$ as it follows:

$$\begin{aligned}
& \left[m_{buoy} + \rho L_{pipe2} A_{pipe2} \left(\frac{D_p}{D_{pipe2}} \right)^2 \right] \ddot{z} \\
& + \left[\frac{1}{2} \rho f A_p \frac{L_{pipe2}}{D_{pipe2}} \left(\frac{D_p}{D_{pipe2}} \right)^2 \right] |\dot{z}| \dot{z} = -F_W
\end{aligned} \quad (13)$$

In the other case, (buoy completely immersed in water), the rising phase is characterized by the following equation:

$$\begin{aligned}
& \left[m_{buoy} + m_{add3} + \rho L_{pipe1} A_{pipe1} \left(\frac{D_p}{D_{pipe1}} \right)^2 \right] \ddot{z} \\
& + b_3 \dot{z} + \left[\frac{1}{2} \rho C_D S_w + \frac{1}{2} \rho f A_p \frac{L_{pipe1}}{D_{pipe1}} \left(\frac{D_p}{D_{pipe1}} \right)^2 \right] |\dot{z}| \dot{z} \\
& \times \dot{z} = \rho g V_{buoy} - F_p - F_W
\end{aligned} \quad (14)$$

where the pressure force F_p and the weight force F_W act, while the Archimede's force $\rho g V_{buoy}$ substitutes the

exciting force. The draft equals the height of the buoy ($D = H_{buoy}$), while m_{add3} and b_3 are evaluable by considering the same draft during rising and falling, by referring ever to the graphs of Figure 6A,B. During the falling phase, only the weight force acts, the motion equation is given by:

$$\begin{aligned}
& \left[m_{buoy} + m_{add3} + \rho L_{pipe2} A_{pipe2} \left(\frac{D_p}{D_{pipe2}} \right)^2 \right] \ddot{z} + b_3 \dot{z} \\
& + \left[\frac{1}{2} \rho C_D S_w + \frac{1}{2} \rho f A_p \frac{L_{pipe2}}{D_{pipe2}} \left(\frac{D_p}{D_{pipe2}} \right)^2 \right] |\dot{z}| \dot{z} \\
& = \rho g V_{buoy} - F_W
\end{aligned} \quad (15)$$

The combined solution of Equations (10), (11), (12), (13), (14), and (15) will provide the vertical motion of the buoy, and, consequently, the excursion of the buoy.

Unfortunately, it is very hard to combine these equations and to obtain the overall solution over time in closed-form. In fact, it must be observed that:

1. When the wave rises (line magenta in Figure 7), the nonreturn valve of the delivery pipe opens and the bottom of the buoy, initially sunk of $z_A + z_w$, starts to rise until it reaches the maximum position (see line cyan in Figure 7). During this phase, corresponding to the useful work of the pump, when the power is delivered to the system, the motion is described by differential Equation (10).
2. At this point, the stroke of the piston pump ends and the nonreturn valve of the delivery pipe closes (Figure 2), so that the force F_p stops acting, the power take off force is only the weight force F_W and Equation (11) becomes the motion equation.
3. The buoy cannot go down and its bottom level remains unchanged (see Figure 7) until the resultant of the forces in Equation (11) provides an acceleration toward the bottom (see Figures 5 and 7).
4. The wave drags the buoy downward until it reaches the minimum position. During this phase (filling phase), the pump sucks water from the tank highlighted in Figure 1A,B at atmospheric pressure, while the nonreturn valve of the blue circuit remains open—see Figure 2.
5. After reaching the minimum position, the buoy cannot rise until the resultant forces in Equation (10) provide an acceleration upward the top (see Figure 7), being the excitation force able to win the pressure and the weight forces and to open the nonreturn valve of the delivery circuit.
6. The buoy restarts to go up and the previous phases are cyclically repeated.

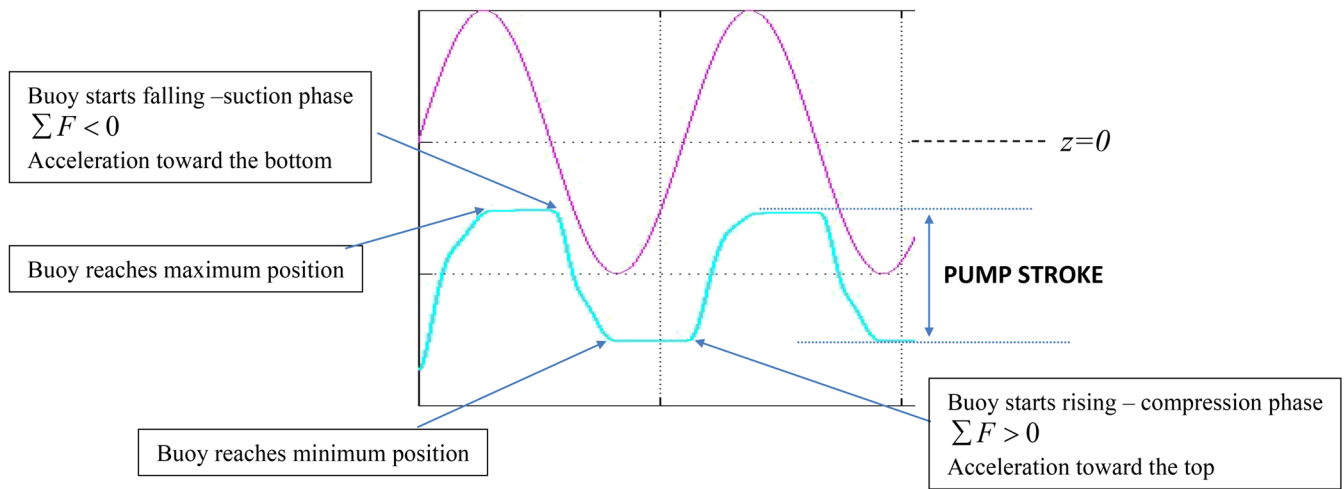


FIGURE 7 Trend of the wave and buoy motion over time along the vertical direction z [Colour figure can be viewed at wileyonlinelibrary.com]

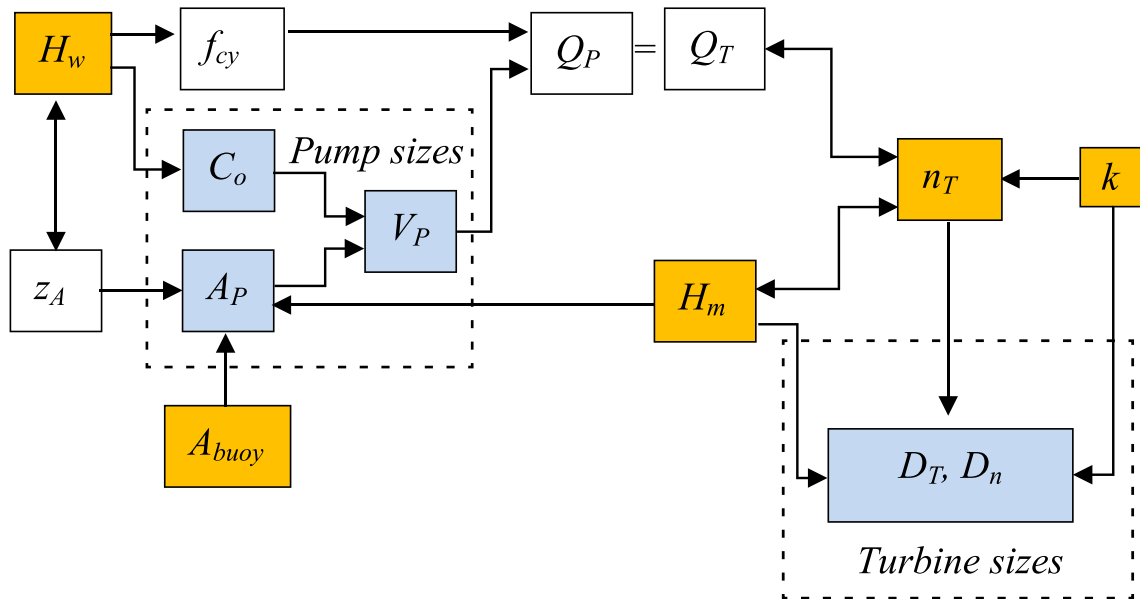


FIGURE 8 Sizing procedure scheme [Colour figure can be viewed at wileyonlinelibrary.com]

The stroke of the piston pump (C_o) is highlighted in Figure 7; however, a rigorous and complete mathematical formulation is hard to obtain, because of the inertial phenomena and the transients of the various phases. For this reason, the differential equations (10), (11), (12), (13), (14), and (15) have been implemented in a Matlab-Simulink @ code, which takes into account all the phases described above in a complete buoy oscillation.

3.2 | Sizing procedure overview

The flowchart depicted in Figure 8 describes an overview of the design procedure, where the wave height (H_w),

the buoy area (A_{buoy}), the reservoir pressure (H_m), and the rated rotational speed (n_T) of the Pelton Turbine, represent the input, highlighted in the orange boxes. The blue boxes contain all other derived devices/parameters (output). In particular, the height of the wave determines the number of cycles per minute, N_{cy} , and the stroke, C_o , of the pump.

The area of the piston, A_p , or its diameter, D_p , is determined by the pressure force F_p , which depends on the pressure of the reservoir (see Equation (6)). Anyway, this area must be lower than the buoy area (A_{buoy}) and such that the consequent sinking z_A (see Equation (8)) is lower than the height of the wave.

The displacement of the pump, V_p , is then found and, accordingly, the flow rate, Q_p , is determined. The

continuity equation imposes the same flow rate to the turbine (Q_T). Finally, the diameter of the Pelton turbine, D_T , is obtained, by considering the nominal pressure, $\rho g H_m$, of the reservoir, together with the nominal rotation speed of the turbine, n_T .

The next paragraphs explain in more detail how sizing the buoy, the piston pump, the reservoir and the Pelton Turbine.

3.2.1 | Size of the buoy

A key design parameter is the wave height. As displayed in the flow chart of Figure 8, this parameter is fundamental for sizing the overall system.

The maximum “capture width” or “absorption width”, L_{\max} is calculable by considering the maximum energy that may be absorbed by a heaving axisymmetric body equals the wave energy transported by the incident wave front of width equal to the wavelength divided by 2π .²⁰

Therefore, it is defined as it follows²¹:

$$L_{\max} = \frac{\lambda}{2\pi} \quad (16)$$

where the wave length is defined as:

$$\lambda = \frac{gT_e^2}{2\pi} \quad (17)$$

Then, the maximum wave power, P_{\max} , absorbed by a heaving axisymmetric body can be given as follows:

$$P_{\max} = J L_{\max} \quad (18)$$

being J is the energy flux per unit width of wave front, which, for deep-water linear waves, is given by:

$$J = \frac{\rho g^2 T H_w^2}{32\pi} \quad (19)$$

$$J = \frac{\rho g^2 T_e H_s^2}{64\pi} \quad (20)$$

In the last two equations, ρ is the water density, T and H_w are the period and height of a regular wave, instead T_e and H_s (significant wave height evaluated as the mean wave height trough to crest of the highest third of the waves— $H_{1/3}$) refer to waves in the real sea. Following Twidell and Weir,²² for successful devices, it should be satisfied the expression:

$$CWR = \frac{L_{\max}}{D_B} \geq 3 \quad (21)$$

where D_B is the size of a cylindrical buoy.

Anyway, a practical rule recommends the point absorber diameter D_B should preferably be in the range of 5% to 10% of the prevailing wavelength.²³

3.2.2 | Piston pump

It is very important to size correctly the geometrical parameters of the piston pump (stroke C_o , piston area A_p , diameter D_p), because its volume determines the flow rate Q_p .

In fact, taking into account this volume V_p and considering the characteristic frequency of the wave, $f_{cy} = 1/T_e$, the flow rate can be provided by the following equation:

$$Q_p = V_p f_{cy} = \frac{A_p C_o}{T_e} \quad (22)$$

The sizing of the piston Area, A_p , is strictly correlated to the sizing of the buoy because of their direct connection: it is obtained by considering the equilibrium in the steady condition (still sea), by means of Equations (6) and (8), as it follows:

$$F_p = \frac{\rho g H_m}{\eta_p} A_p = \rho g z_A A_{buoy} \quad (23)$$

By simplifying:

$$A_p = \eta_p z_A \frac{A_{buoy}}{H_m} \quad (24)$$

The choice of the pressure of the reservoir (indicated equivalently as p_{res} or H_m —column water meters) is linked to the Pelton turbine design and it is described in the next section.

3.2.3 | Reservoir

The design of the reservoir is obtained by determining its volume. The pressure of the reservoir, H_m , is guaranteed by the presence of an air mass, which is compressed so that its volume changes as it follows:

$$V_{air} = \frac{m_{air} \bar{R} T_{air}}{\rho_{water} g H_m} \quad (25)$$

The pressure oscillations are determined, by considering an isothermal compression, as:

$$(H_m + \Delta H_m)(V_{air} - \Delta V) = V_{air}H_m \quad (26)$$

or in different way:

$$\frac{\Delta H_m}{H_m} = \frac{\Delta V}{V_{air} - \Delta V} \quad (27)$$

where the quantity ΔV is the volume transited in the unit of time, numerically equal to the flow rate provided by the piston pump. It is therefore possible to use an adequate air mass m_{air} , to reduce the amplitude of these oscillations to an acceptable value. The choice of the air mass is then conditioned by the necessity to design a volume of the reservoir with limited sizes.

3.2.4 | Micro Pelton turbine

The selection of the Pelton turbine is given taking into account the pressure level of the reservoir and the specific speed, defined as:

$$k = \frac{2\pi n_T}{60} \frac{\sqrt{Q}}{(gH_m)^{0.75}} \quad (28)$$

whose optimal range is [0-0.18].

Therefore, the Pelton turbine nominal flow rate, by considering the nominal pressure of the reservoir, H_m , can be determined as:

$$Q_T = \frac{k^2 g^{1.5} H_m^{1.5}}{\left(\frac{2\pi n_T}{60}\right)^2} \quad (29)$$

At maximum efficiency conditions, it results that:

$$u \cong 0.5c_0 = 0.5\varphi_v \sqrt{2gH_m} \quad (30)$$

where

$$c_0 = \varphi_v \sqrt{2gH_m} \quad (31)$$

is the spouting velocity of the jet, u is the peripheral velocity and φ_v a velocity reduction coefficient.

The peripheral velocity depends on the Pelton turbine diameter D_T as follows:

$$u = \frac{\pi D_T n_T}{60} \quad (32)$$

Therefore, by considering the nominal pressure of the reservoir, H_m , depending on Equation (24), the turbine diameter is expressed as:

$$D_T = \frac{30\varphi_v}{\pi n_T} \sqrt{2gH_m} = 42.2 \frac{\varphi_v}{n_T} \sqrt{H_m} \quad (33)$$

In an analogous way, the nozzle diameter D_n can be determined by considering that the turbine flow rate is expressed as:

$$Q_T = A_n c_0 = \frac{\pi D_n^2}{4} c_0 \quad (34)$$

Then, from Equation (34) it results that:

$$D_n = \sqrt{\frac{4Q_T}{\pi c_0}} \quad (35)$$

It is important to remark that the ratio D_n/D_T has to be lower than 1/8.

3.3 | Control strategy and optimization

With the aim to detect the optimal working conditions of the system, for each wave height, it is necessary to obtain the optimal value of the power. The power depends on many parameters and it is necessary to find which of them to optimize.

For calculating the power of the system, one considers that the wave energy is converted into electrical power through the pump and the turbine working. The power supplied by the pump equals that delivered by the Pelton turbine, reduced by the turbine losses, so that one obtains:

$$P_T = \eta_T \rho g Q_T H_m \quad (36)$$

The flow rate of the turbine, Q_T , must coincide with the pump one, Q_P , obtained from Equation (22), as product between the volume of the pump, and the wave frequency. The volume of the piston pump is determined by the stroke C_o , whose values are given by differential equations (10) to (15). The solution of the differential equations is very complicated, so in the next paragraph some simplified formulas about the stroke of the piston pump are introduced.

3.3.1 | Stroke of the piston pump

The two formulas of the stroke, solutions of Equations (10) and (11), by considering the rising phase and the falling phase separately, can be written as follows:

$$C_o(t) = \frac{C_{o1}}{2} \sin(\omega t + \varphi_1) \quad (37)$$

$$C_o(t) = \frac{C_{o2}}{2} \sin(\omega t + \varphi_2) \quad (38)$$

By substituting these formulas, evaluated at the times corresponding to the maximum and minimum of the wave, $t = \pi/2\omega$ and $t = 3\pi/2\omega$, in Equations (10) and (11), one obtains the amplitude of the sinusoids $C_{o1}/2$ and $C_{o2}/2$ whose sum is equal to the entire stroke C_0 . Therefore, by substituting in Equations (10) and (11), the terms $\frac{C_{o1}}{2} \sin(\frac{\pi}{2} + \varphi_1)$ and $\frac{C_{o2}}{2} \sin(\frac{3\pi}{2} + \varphi_2)$, with their derivatives one obtains:

$$\begin{aligned} & -\frac{C_{o1}}{2} \left[\frac{m_{buoy} + m_{add1} + \rho L_{pipe1} A_{pipe1} \left(\frac{D_p}{D_{pipe1}}\right)^2}{\rho g A_{buoy}} \right] \omega^2 \\ & - \frac{C_{o1}}{2} \frac{b1}{\rho g A_{buoy}} \omega \tan(\varphi_1) - \left[\frac{\frac{1}{2} \rho C_{D1} S_w + \frac{1}{2} \rho f A_p \frac{L_{pipe1}}{D_{pipe1}} \left(\frac{D_p}{D_{pipe1}}\right)^2}{\rho g A_{buoy}} \right] \\ & \times \omega^2 \tan(\varphi_1) \sin(\varphi_1) + \frac{C_{o1}}{2} = \frac{H_w}{2} - \frac{z_A + z_w}{\cos(\varphi_1)} \end{aligned} \quad (39)$$

$$\begin{aligned} & \frac{C_{o2}}{2} \left[\frac{m_{buoy} + m_{add2} + \rho L_{pipe2} A_{pipe2} \left(\frac{D_p}{D_{pipe2}}\right)^2}{\rho g A_{buoy}} \right] \omega^2 \\ & + \frac{C_{o2}}{2} \frac{b2}{\rho g A_{buoy}} \omega \tan(\varphi_2) + \left[\frac{\frac{1}{2} \rho C_{D2} S_w + \frac{1}{2} \rho f A_p \frac{L_{pipe2}}{D_{pipe2}} \left(\frac{D_p}{D_{pipe2}}\right)^2}{\rho g A_{buoy}} \right] \\ & \times \omega^2 \tan(\varphi_2) \sin(\varphi_2) - \frac{C_{o2}}{2} = -\frac{H_w}{2} - \frac{z_w}{\cos(\varphi_2)} \end{aligned} \quad (40)$$

The phases φ_1 and φ_2 are calculable as:

$$\tan \varphi_{1,2} = \frac{2\gamma_{1,2}\omega}{\omega^2 - \omega_{01,2}^2} \quad (41)$$

In Equation (41), the natural frequency is calculable as:

$$\omega_{01,2}^2 = \frac{\rho g A_{buoy}}{m_{buoy} + m_{add1,2} + \rho L_{pipe1,2} A_{pipe1,2} \left(\frac{D_p}{D_{pipe1,2}}\right)^2} \quad (42)$$

while the damping ratio is given by:

$$2\gamma_{1,2} = \frac{b_{1,2} + \left(\frac{1}{2} \rho C_{D1,2} S_w + \frac{1}{2} \rho f A_p \frac{L_{pipe1,2}}{D_{pipe1,2}} A_{pipe1,2} \left(\frac{D_p}{D_{pipe1,2}}\right)^2 \right) |\dot{z}|}{m_{buoy} + m_{add1,2} + \rho L_{pipe1,2} A_{pipe1,2} \left(\frac{D_p}{D_{pipe1,2}}\right)^2} \quad (43)$$

Usually, these phases (see Equation (41)) are small. In fact, the natural frequency ω_0 is greater than the waves frequencies, being necessary to increase the area of the buoy in order to capture as much energy as possible. For this reason, in a first rough analysis, the phases are put equal to zero.

In such a way, by combining Equations (39) and (40), the stroke of the piston pump becomes:

$$\begin{aligned} & \frac{C_{o1}}{2} - \frac{C_{o1}}{2} \left[\frac{m_{buoy} + m_{add1} + \rho L_{pipe1} A_{pipe1} \left(\frac{D_p}{D_{pipe1}}\right)^2}{\rho g A_{buoy}} \right] \omega^2 \\ & + \frac{C_{o2}}{2} - \frac{C_{o2}}{2} \left[\frac{m_{buoy} + m_{add2} + \rho L_{pipe2} A_{pipe2} \left(\frac{D_p}{D_{pipe2}}\right)^2}{\rho g A_{buoy}} \right] \\ & \times \omega^2 = H_w - z_A \end{aligned} \quad (44)$$

By simplifying, one obtains:

$$\frac{C_{o1}}{2} \left[1 - \left(\frac{\omega}{\omega_{01}} \right)^2 \right] + \frac{C_{o2}}{2} \left[1 - \left(\frac{\omega}{\omega_{02}} \right)^2 \right] = H_w - z_A \quad (45)$$

Finally, by approximating ω_{01} and ω_{02} to ω_0 defined as:

$$\omega_0^2 = \frac{\rho g A_{buoy}}{m_{buoy} + \overline{m_{add}} + \rho \overline{L_{pipe}} \overline{A_{pipe}} \left(\frac{D_p}{D_{pipe}}\right)^2} \quad (46)$$

where the terms $\overline{m_{add}}$, $\overline{L_{pipe}}$, $\overline{D_{pipe}}$, represent average values, this simple equation is achieved:

$$\frac{C_{o1}}{2} + \frac{C_{o2}}{2} = C_0 = \frac{H_w - z_A}{1 - \left(\frac{\omega}{\omega_0}\right)^2} = \frac{H_w - z_A}{1 - \left(\frac{2\pi}{T_e \omega_0}\right)^2} \quad (47)$$

3.3.2 | Power of the system in optimal conditions

The following analysis considers sea states characterized by wave periods as estimated by Moskowitz¹²:

$$T_e = 5\sqrt{H_w} \quad (48)$$

By involving the electrical efficiency and taking reference to Equations (22), (24), and (47), it is possible to calculate the power of the system, as it follows:

$$P_{System} = \eta_{el}\eta_T\rho g Q_T H_m = \eta_{el}\eta_T\rho g Q_P H_m = \eta_{el}\eta_T\rho g \frac{A_p C_o}{5\sqrt{H_w}} H_m$$

$$= \frac{\eta_{el}\eta_p\eta_T\rho g A_{buoy} z_A}{5\sqrt{H_w}} \frac{(H_w - z_A)}{\left[1 - \frac{4}{25H_w} \left(\frac{\pi}{\omega_0}\right)^2\right]} \quad (49)$$

By deriving respect to z_A and putting equal zero the derivative, the maximum power is obtained for $z_A = H_w/2$. Therefore, by considering Equation (47) the optimal stroke is:

$$(C_o)_{opt} = \frac{H_w}{2 \left[1 - \frac{4}{25H_w} \left(\frac{\pi}{\omega_0}\right)^2\right]}, \quad (z_A)_{opt} = \frac{H_w}{2} \quad (50)$$

At this point, by considering that the sinking z_A is correlated to the pressure of the reservoir (see Equations (8) and (24)) as:

$$z_A = \frac{A_p p_{res}}{\rho g \eta_p A_{buoy}} \quad (51)$$

it is possible to obtain two main equations.

The first equation links the power of the system to the height of the wave and to the pressure of the reservoir:

$$P_{System} = \eta_{el}\eta_T p_{res} A_p \frac{\left(H_w - \frac{A_p p_{res}}{\rho g \eta_p A_{buoy}}\right)}{5\sqrt{H_w} \left[1 - \frac{4}{25H_w} \left(\frac{\pi}{\omega_0}\right)^2\right]} \quad (52)$$

The second one is written considering optimal conditions: in this case the sinking z_A is equal to half height of the wave. The power of the overall system, by rewriting Equation (49) in optimal conditions, could be so estimated as it follows:

$$(P_{System})_{opt} = \frac{5}{4} \left[\frac{\eta_{el}\eta_p\eta_T\rho g A_{buoy} H_w^{2.5}}{25H_w - 4 \left(\frac{\pi}{\omega_0}\right)^2} \right] \quad (53)$$

This simple equation shows that the power of the system depends, in optimal conditions and at the peak frequencies, on the height of the wave and on the area of the buoy. By remembering that the optimal conditions

are those which determine a sinking z_A equal to half of the height of the wave, by considering Equations (50) and (51), the pressure which guarantee that is given by the following formula:

$$(p_{res})_{opt} = \frac{H_w \rho g \eta_p A_{buoy}}{2 A_p} \quad (54)$$

Then, the optimal pressure of the reservoir, once fixed the system geometrical parameters, depends on the height of the wave.

3.3.3 | Sizing of the turbine nozzle

The system has the possibility to work always in optimal conditions by changing the pressure of the reservoir. The law of continuity imposes that:

$$Q_T = Q_P \quad (55)$$

Taking into account Equations (22), (47), and (48), the flow rate of the pump, can be expressed as:

$$Q_P = \frac{V_P}{T_e} = \frac{C_o A_p}{T_e} = \frac{(H_w - z_A) A_p}{T_e \left[1 - \frac{4}{25H_w} \left(\frac{\pi}{\omega_0}\right)^2\right]}$$

$$= \frac{\left(H_w - \frac{A_p H_m}{\eta_p A_{buoy}}\right) A_p}{5\sqrt{H_w} \left[1 - \frac{4}{25H_w} \left(\frac{\pi}{\omega_0}\right)^2\right]} \quad (56)$$

The Pelton turbine has the possibility of changing its flow rate without efficiency losses, by moving the needle of the nozzle and changing the area of the nozzle, A_n .

Taking into account Equations (31) and (34), the flow rate of the turbine can be expressed as:

$$Q_T = A_n c_0 = A_n \varphi_v \sqrt{2gH_m} \quad (57)$$

Generally, the changes of flow rate are given or by changing the pressure of the reservoir H_m , or the area of the nozzle A_n (see Equation (57)).

However, in the present case, the flow rate of the turbine Q_T is determined by that of the piston pump Q_P . By substituting Equations (56) and (57) in Equation (55), one obtains:

$$A_n \varphi_v \sqrt{2gH_m} = \frac{\left(H_w - \frac{A_p H_m}{\eta_p A_{buoy}}\right) A_p}{5\sqrt{H_w} \left[1 - \frac{4}{25H_w} \left(\frac{\pi}{\omega_0}\right)^2\right]} \quad (58)$$

The nozzle area A_n depends on to the pressure of the reservoir H_m and to the height of the wave H_w . In optimal conditions, taking into account Equation (54), the nozzle area A_n is evaluable as:

$$(A_n)_{opt} = \frac{A_p^{1.5}}{10\varphi_v \left[1 - \frac{4}{25H_w} \left(\frac{\pi}{\omega_0} \right)^2 \right] \sqrt{g\eta_p A_{buoy}}} \quad (59)$$

This equation indicates that there will be an optimum opening of the feeding nozzle of the Pelton turbine, weakly dependent on the waves heights (H_w) variations.

Therefore, once setting the right value of the area of the feeding nozzle of the Pelton turbine, the pressure of the reservoir changes automatically in relation of the height of the wave, by guaranteeing the optimal conditions.

3.3.4 | Sizing procedure by steps

In Figure 9, is reported the sizing procedure organized by steps. First of all is necessary to define the nominal height wave. This fundamental design parameter will determine the period Te , according with Equation (48); then, the size of the buoy as explained in Section 3.2.1. The sinking z_A is linked to the height of the wave design as in Equation (50). For the present purposes the buoy is chosen rectangular shaped whose width is calculated as 10% of the wave design length. At this point it is necessary to choose the piston diameter D_p and its area A_p . This parameter allows calculating the flow rate of the pump, as in Equation (22), taking into account the wave period Te . The optimal pressure of the reservoir is provided by Equation (54). Therefore, it is possible, by means of Equation (33), to determine the turbine diameter D_T , after having set its speed number n_T . Finally it is necessary to check if the specific speed of the turbine, provided by Equation (28), falls in the range [0.08-0.18]. In that occurrence is not verified, one can choose another piston diameter until the condition of the specific speed is satisfied.

3.3.5 | Control strategy

Consider that the sea becomes wavy, and the waves are those of design (nominal condition). When the pump starts working, under the waves action, the nozzle feeding the turbine is still closed. The water level in the reservoir rises until the pressure reaches the design value.

For guaranteeing this pressure value, a certain air mass at environment temperature, which at atmospheric

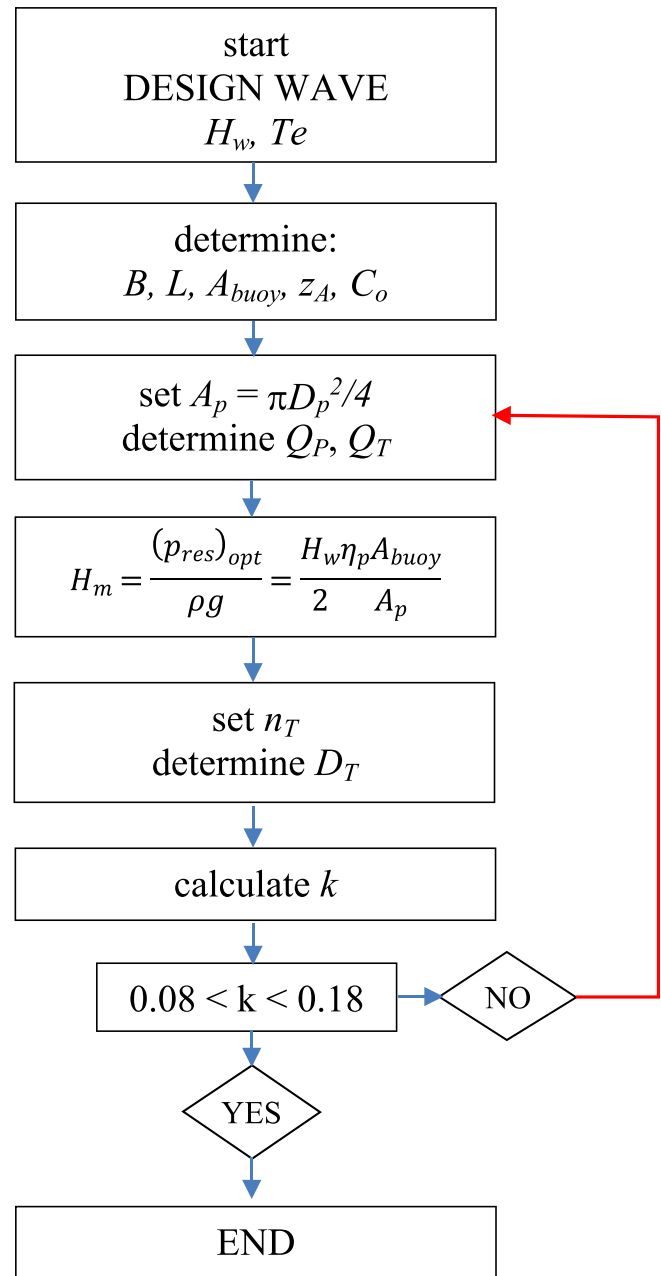


FIGURE 9 Sizing flow chart [Colour figure can be viewed at wileyonlinelibrary.com]

pressure largely fills a reservoir designed with a volume V_{res} , is compressed by the remaining part of water of the reservoir, occupying a final volume V_{fin} .

At this point, the nozzle of the turbine opens and the incoming flow rate is discharged on the turbine itself. The optimal opening is given by Equation (59).

Taking into account that, at nominal conditions, the pump flow rate is evaluated as in Equation (22), while the power provided by the Pelton turbine is given by Equation (53), the pressure oscillations are given by Equation (27).

The volume of the reservoir is sized in such a way that these oscillations are contained at values lower than 5%.

The successive increasing of the height of the waves implies an increased flow rate of the piston pump. By changing the flow rate of the pump, the pressure of the reservoir changes consequently, because of the income of more water in the reservoir, which crushes further the air volume.

At maximum wave height, the pressure of the reservoir reaches the maximum value and the air volume is compressed until the minimum value.

At this point, it is worth pointing out that the efficiency of the turbine would not be the maximum. In fact, the efficiency expression is equal to:

$$\eta_T = 2\varphi_v^2(1 + \psi \cos\beta) \frac{u}{c_o} \left(1 - \frac{u}{c_o}\right) \quad (60)$$

which finds a maximum value for $u/c_o = 0.5$.

If the is the spouting velocity of the jet (see Equation (31)) changes with the pressure level H_m , the peripheral velocity u has to change according. That can be done, by changing the rotational regime as in Equation (32).

Finally, when the wave motion stops and the sea is still, the reservoir does not receive more water. In this condition the reservoir starts emptying. The water mass,

flowing through the nozzle, lowers its level and the reservoir pressure decreases. Under a certain level, the turbine nozzle is closed and the reservoir remains filled partly by water and partly by air, by waiting until the sea becomes wavy again.

4 | APPLICATION OF THE NUMERICAL MODEL FOR CALCULATING THE BUOY OSCILLATIONS

This section describes the main results obtained from the simulations of the software, developed in Matlab Simulink@ environment, which provides the oscillations of the buoy by changing the operating conditions. The code has been applied in different cases, by varying the height of the wave (H_w), the pressure force F_p , the weight force F_w and the wave period T . The simulations refer a buoy area of 12 m^2 . The next figures, from Figures 10 to 13, report some simulations by considering the height of the wave H_w variable from 0.5 to 2 m with step of 0.5 m, the period T of the wave variable from 3.5 to 7 seconds and the pressure force F_p variable from 26.4 to 105.8 kN.

Table 1 reports the main results of the above-illustrated simulations, in term of stroke of the pump, sinking of the buoy z_A and z_W . The simulations, carried

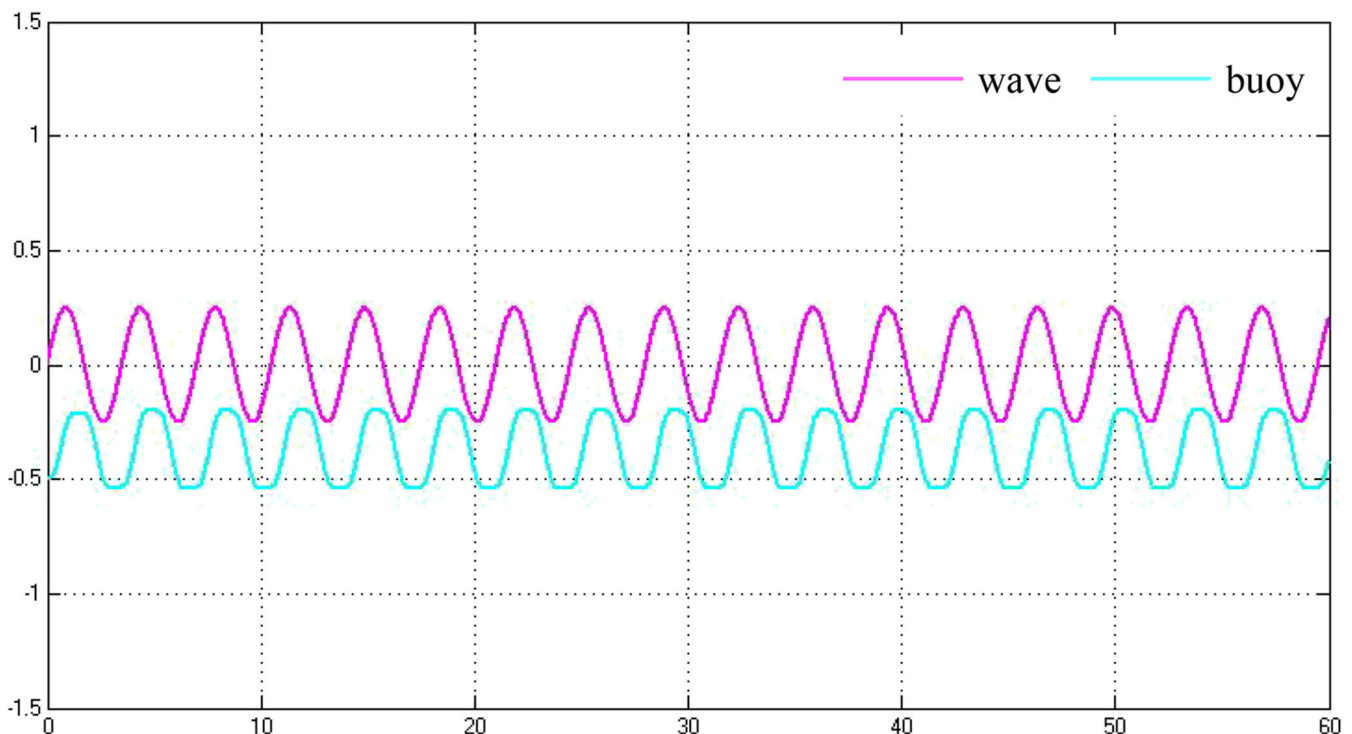


FIGURE 10 Trend of the wave and of the buoy oscillations. $H_w = 0.5 \text{ m}$, $F_p = 26\,460 \text{ N}$, $F_w = 29\,400 \text{ N}$, $T = 3.5 \text{ seconds}$ [Colour figure can be viewed at wileyonlinelibrary.com]

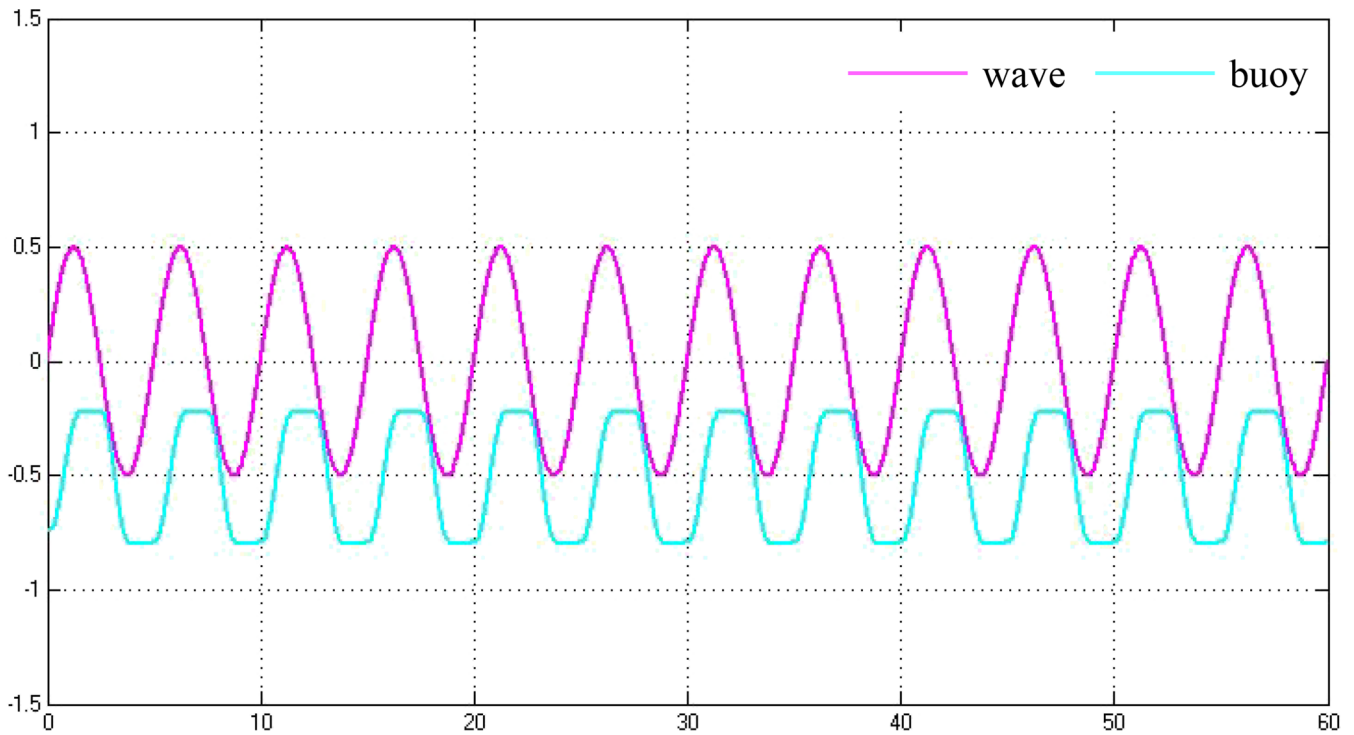


FIGURE 11 Trend of the wave and of the buoy oscillations. $H_w = 1$ m, $F_p = 52\,920$ N, $F_w = 29\,400$ N, $T = 5$ seconds [Colour figure can be viewed at wileyonlinelibrary.com]

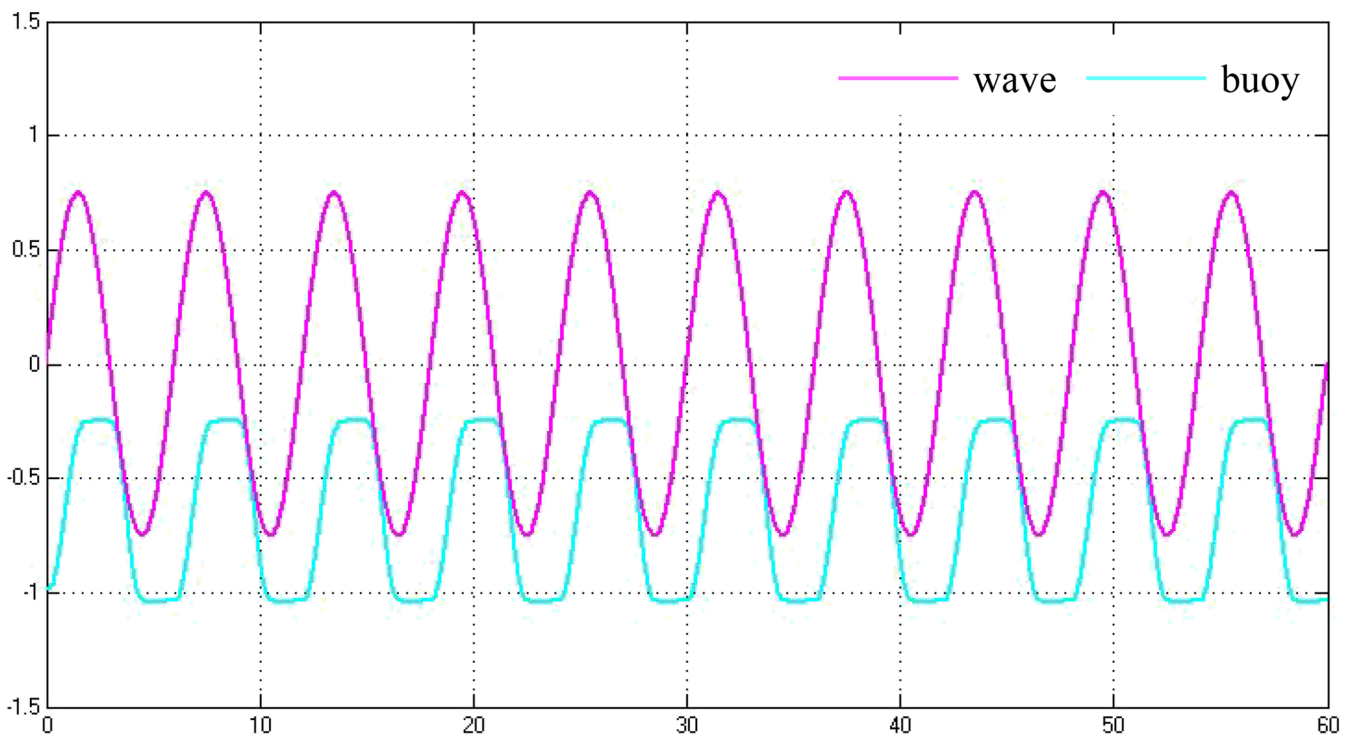


FIGURE 12 Trend of the wave and of the buoy oscillations. $H_w = 1.5$ m, $F_p = 79\,380$ N, $F_w = 29\,400$ N, $T = 6$ seconds [Colour figure can be viewed at wileyonlinelibrary.com]

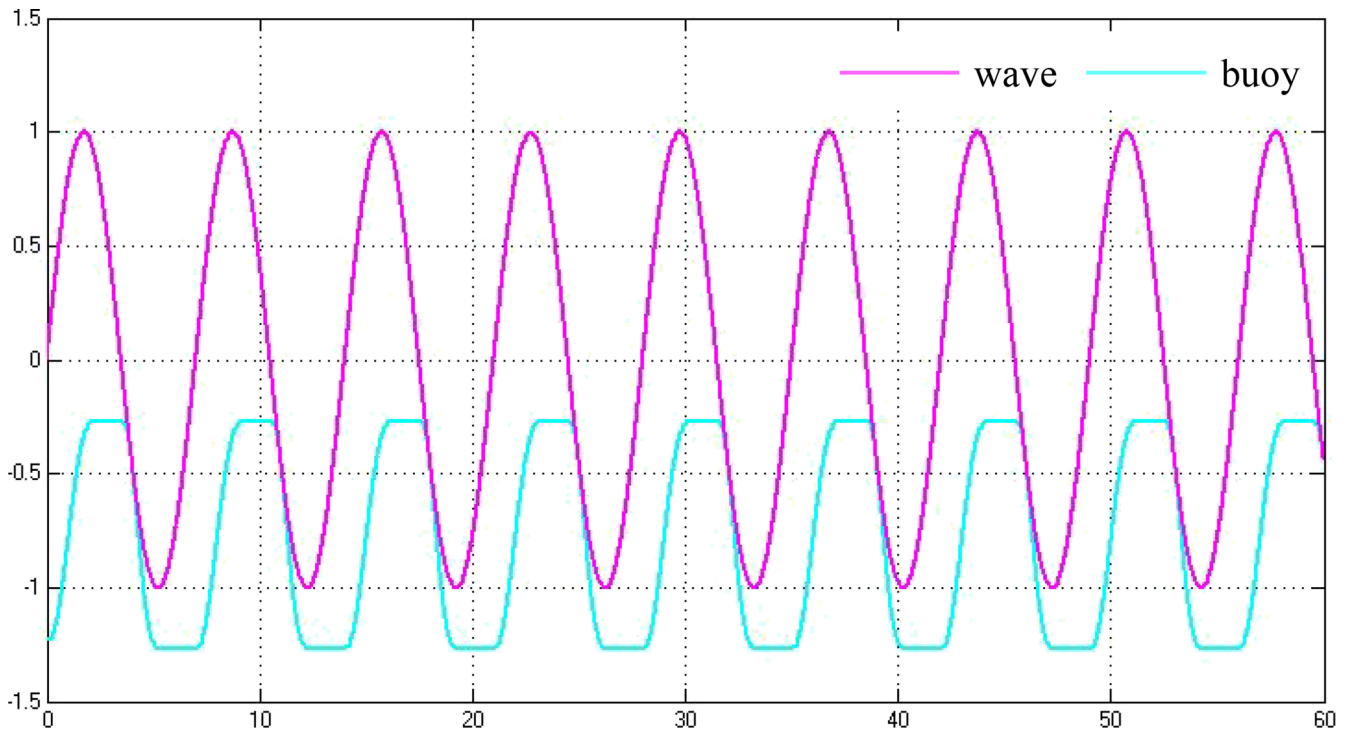


FIGURE 13 Trend of the wave and of the buoy oscillations. $H_w = 2$ m, $F_p = 105\,840$ N, $F_w = 29\,400$ N, $T = 7$ seconds [Colour figure can be viewed at wileyonlinelibrary.com]

TABLE 1 Simulations results

Input				Output			
H_w (m)	F_p (N)	F_w (N)	T (s)	C_o (m) Simulink	z_A (m)	z_w (m)	C_o (m)—Equation (47)
0.5	26 460	29 400	3.5	0.33	0.25	0.25	0.33
1.0	52 920	29 400	5.0	0.59	0.49	0.25	0.59
1.5	79 380	29 400	6.0	0.81	0.74	0.25	0.82
2.0	105 840	29 400	7.0	1.03	0.98	0.25	1.07

out in optimal conditions, demonstrate that in all the considered cases the sinking z_A of the buoy is about a half of the height of the wave. Moreover, the stroke of the piston pump agrees with Equation (47)—simplified formula—in all cases (see last column), with errors contained within the range of 2%.

With the aim to emphasize this result, Table 2 reports the variation of the stroke of the piston pump, by changing the pressure force F_p for a wave having height of 1 m and period of 5 seconds.

In Table 2, it is evident that for the lower values of the pressure force the buoy tends to follow the wave oscillations, by determining so a high stroke of the pump.

TABLE 2 Variation of the stroke for $H_w = 1$, $T = 5$ seconds

F_p (N)	C_o (m)	z_A (m)
29 400	0.78	0.27
34 300	0.75	0.32
39 200	0.71	0.36
44 100	0.67	0.41
49 000	0.62	0.45
53 900	0.58	0.50
58 800	0.53	0.55
63 700	0.47	0.59
68 600	0.41	0.64

The opposite happens if the pressure force reaches higher values. In this case, the stroke tends to reduce. Simulations demonstrate that the same behavior occurs by varying the height of the wave.

Since the power delivered by the piston pump is proportional to the product of the two factors, as shown before, there will be an optimal value. Therefore, for obtaining that, it is necessary to set adequately the right

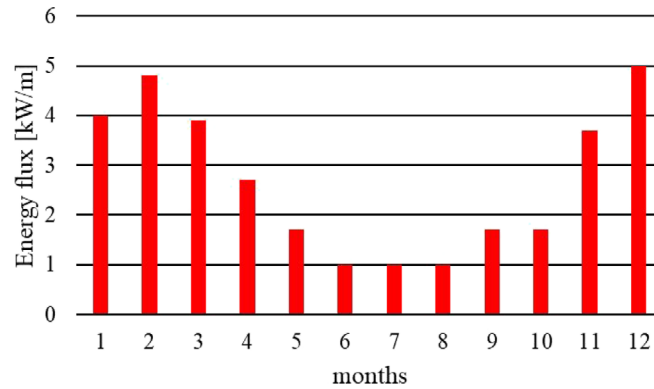


FIGURE 14 Mean monthly flux of energy measured by the buoy station RON of Cetraro (Italy)¹⁹ [Colour figure can be viewed at wileyonlinelibrary.com]

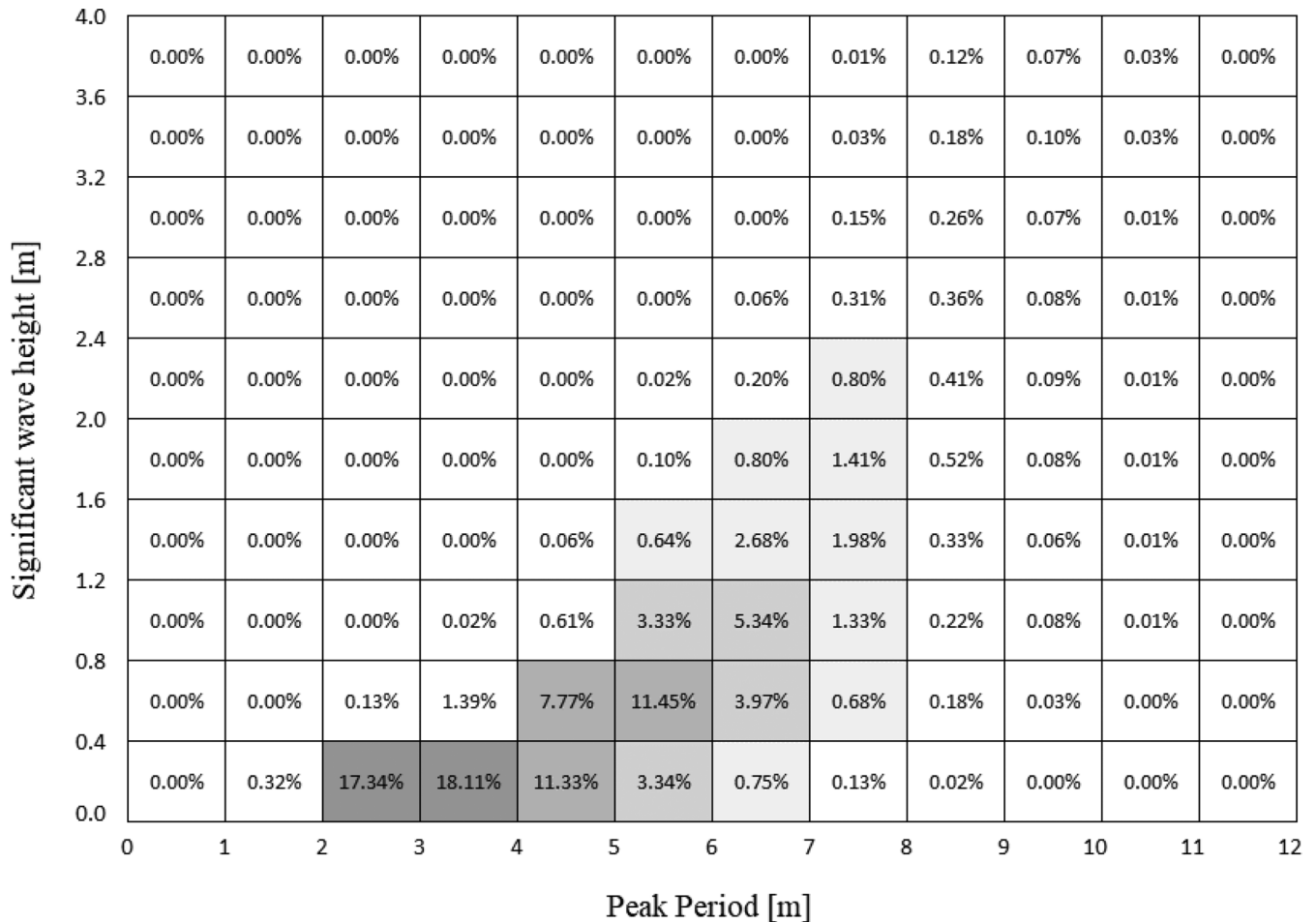


FIGURE 15 Joint Probability distribution (%) for the near shore region of Cetraro (Italy)¹⁹

value of the pressure force, by setting the pressure of the reservoir as illustrated in Equation (54).

5 | STUDY CASE AND RESULTS

In this section, the system is designed for the Calabrian site of Cetraro. Its sizing was performed with the aim of obtaining small dimensions of all the components. The mean monthly energy flux, represented in Figure 14, takes into account the period T and the height H_w registered by a buoy RON installed at Cetraro site¹⁹:

From Figure 14, it is possible to estimate a mean yearly energy flux of 2.7 kW/m: this value is low, compared with other sites, but representative of most of the southern Italian coasts.

Figure 15 reports the probability distribution chart of the wave heights for the near shore region of Cetraro. The chart, developed on a temporal period of 8 years, shows that the 77% of the phenomena are represented by waves having height lower than 0.8 m.²⁶ This implies that the height of the wave to be considered for the nominal conditions of the system (design wave height) is about 0.8 m, suitable for the energy flux distribution of the site.

From this value, and tacking into account the joint probability distribution of Figure 15, it is possible to determine the sizes of the buoy. Starting from the wave height of 0.8 m (wave at which nominal conditions correspond), having a period of 5.75 seconds and a wavelength of 50 m, the maximum capture width must not exceed 8 m (see Equation (16)). Following the criteria exposed in Section 3.2.1, the buoy is chosen having a rectangular body with width B of 4 m (8% of the prevailing wavelength) and length L of 3 m.

5.1 | Sizing of the main component

The sizing of the other components is done following what is exposed in Section 3.3.4 where Figure 9 exhibits a flow chart summarizing the calculation of all the system parameters.

Considering the chosen sizes B and L , the buoy area A_{buoy} is 12 m², while the sinking z_A , computed as the 50% of the nominal wave height, is equal to 0.4 m.

The stroke of the piston pump, is computed as in Equation (47), little more than half of the nominal wave, therefore equal to 0.44 m while the frequency of the nominal wave height, according with,¹² but even taking into account the data of the site¹⁹ is estimated as $f_{cy} = 0.17$ Hz.

By means of Equation (23), the pressure force at nominal conditions will be 47.04 kN. By setting a piston

pump diameter of 0.25 m, one obtains the piston area $A_p = 0.05$ m²; by assuming the system piping efficiency $\eta_p = 0.9$ one obtains the nominal pressure (expressed as water column meters) $H_m = 88$ m.

By employing Equation (33) and establishing the parameters $\varphi_v = 0.98$ and $n_T = 3000$ rpm, the latter pressure value will led to a turbine diameter D_T of 13 cm.

Instead, the pump flow rate, at nominal conditions, will be equal to the pump volume delivered in the unit time, that is, the volume multiplied the wave frequency, which, for the present case, will be equal (ever at nominal conditions) to 3.7 L/s.

Considering the jet velocity $c_o = 40.7$ m/s (see Equation (31)), the nozzle diameter D_n is 1.1 cm. The specific speed k , calculable as in Equation (28) is equal to 0.12, and it falls in the range 0.08-0.18, therefore no iterations are required (see Figure 9).

The system is conceived for working with wave height until 4 m. For this reason, besides the nominal conditions, a maximum stroke of the piston pump, a maximum flow rate, a maximum pressure of the reservoir and

TABLE 3 Input/output parameters of the system

Parameter	Symbol	Value
INPUT		
Wave height (nominal condition)	H_w	0.8 m
Wave period	T_e	5.75 seconds
Wave length	λ	50 m
Buoy width	B_{buoy}	4 m
Buoy length	L_{buoy}	3 m
Buoy area	A_{buoy}	12 m ²
Piston pump diameter	D_P	0.25 m
Piston pump Area	A_P	0.05 m ²
Turbine rotational speed	n_T	3000 rpm
OUTPUT		
Piston pump stroke at nominal condition	C_o	0.44 m
Piston pump length	C_{max}	2 m
Flow rate at nominal condition	Q_P	3.7 L/s
Maximum flow rate	Q_{max}	10.0 L/s
Turbine diameter	D_T	13 cm
Turbine nozzle diameter (maximum opening)	D_n	1.2 cm
Pressure force at nominal condition	F_p	51.7 kN
Pressure of the reservoir at nominal condition	p_{res}	9 Bar
Maximum pressure of the reservoir	p_{res_max}	40 Bar
Maximum rotational regime	n_{Tmax}	6500 rpm

finally a maximum rotational regime are also calculated. In a first rough configuration, all the system input/output parameters are reported in the next table (Table 3). In the

next sections, simulations regarding the piston stroke trend and the power of the system are reported in different conditions.

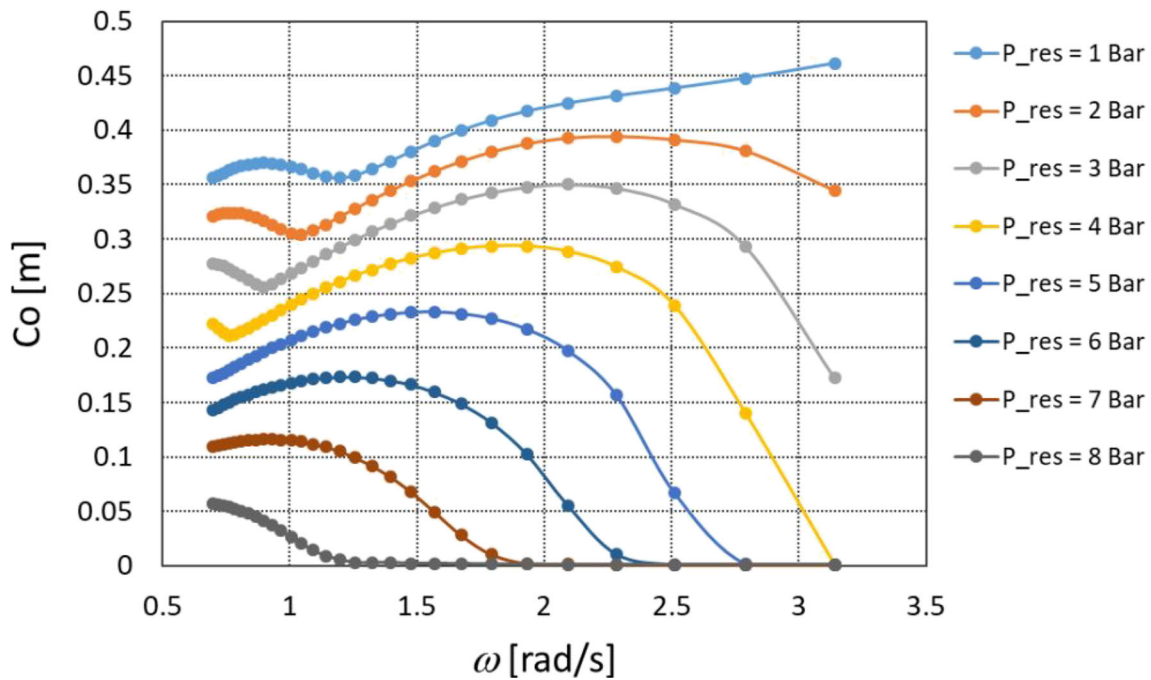


FIGURE 16 Trend of the piston stroke C_o by changing the circular frequency and the pressure of the reservoir, for a wave of 0.4 m height [Colour figure can be viewed at wileyonlinelibrary.com]

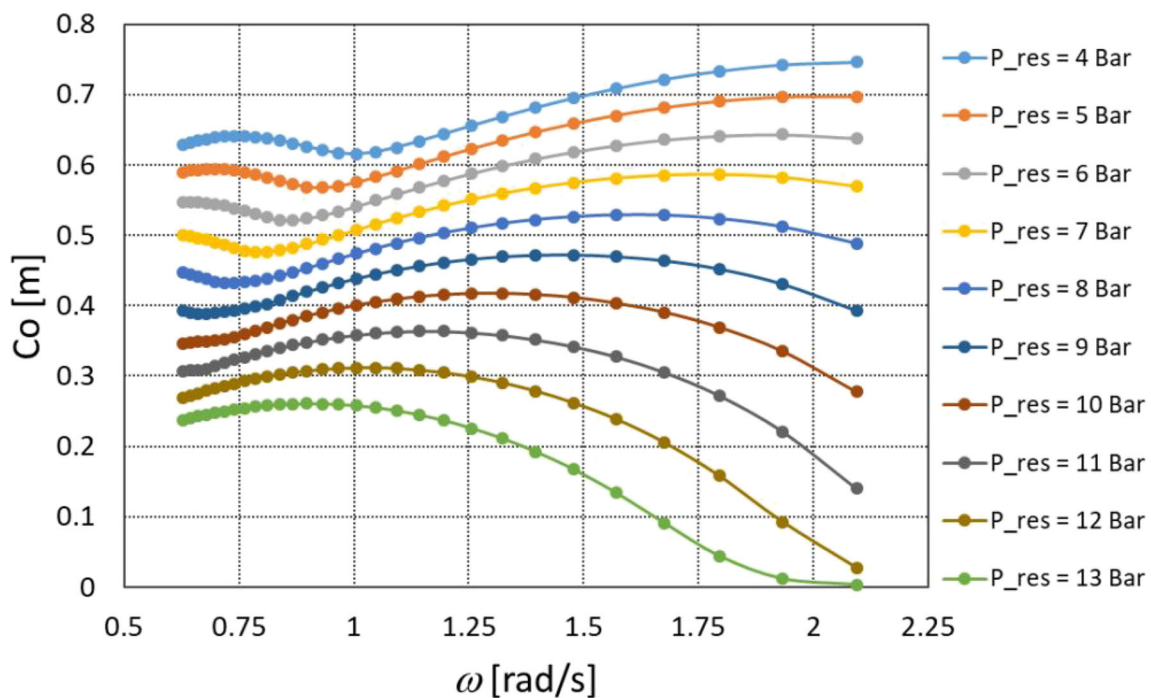


FIGURE 17 Trend of the piston stroke C_o by changing the circular frequency and the pressure of the reservoir, for a wave of 0.8 m height [Colour figure can be viewed at wileyonlinelibrary.com]

5.2 | Piston stroke trend

The following simulations are done by considering the sizing procedure before applied for the site of Cetraro

which led to determine an area of the buoy of 12 m² and an area of the piston pump of 0.05 m². Next figures, from Figures 16 to 20, illustrate the piston stroke, C_o , vs the circular frequency of the wave, by changing the pressure

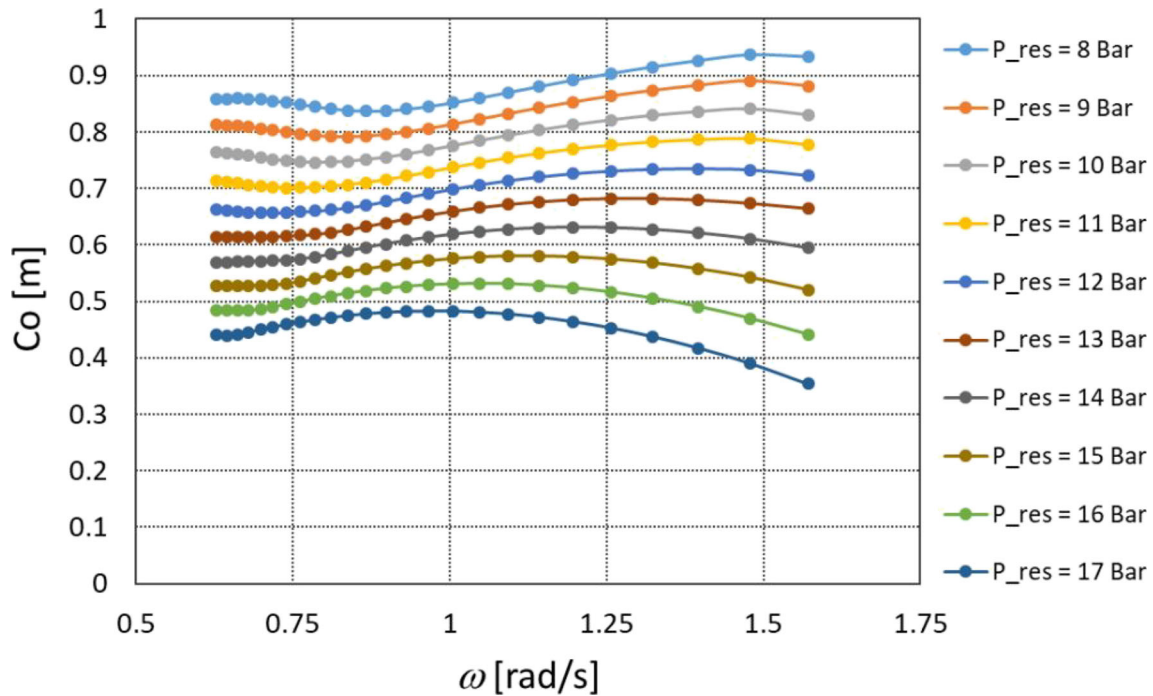


FIGURE 18 Trend of the piston stroke C_o by changing the circular frequency and the pressure of the reservoir, for a wave of 1.2 m height [Colour figure can be viewed at wileyonlinelibrary.com]

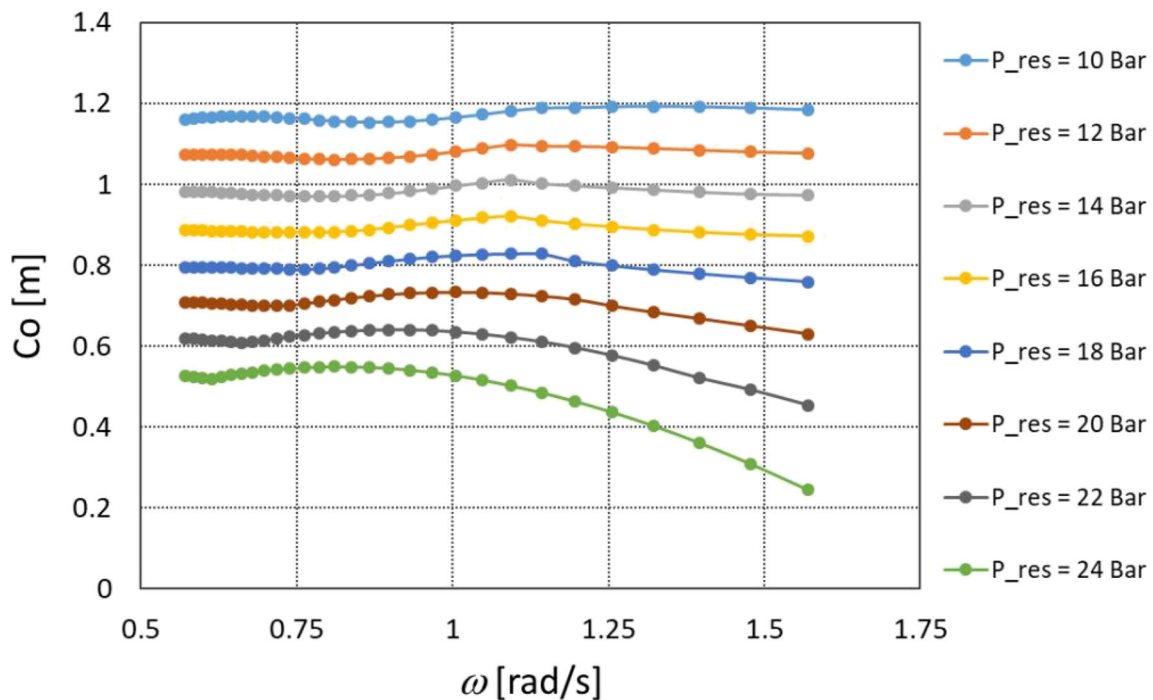


FIGURE 19 Trend of the piston stroke C_o by changing the circular frequency and the pressure of the reservoir, for a wave of 1.6 m height [Colour figure can be viewed at wileyonlinelibrary.com]

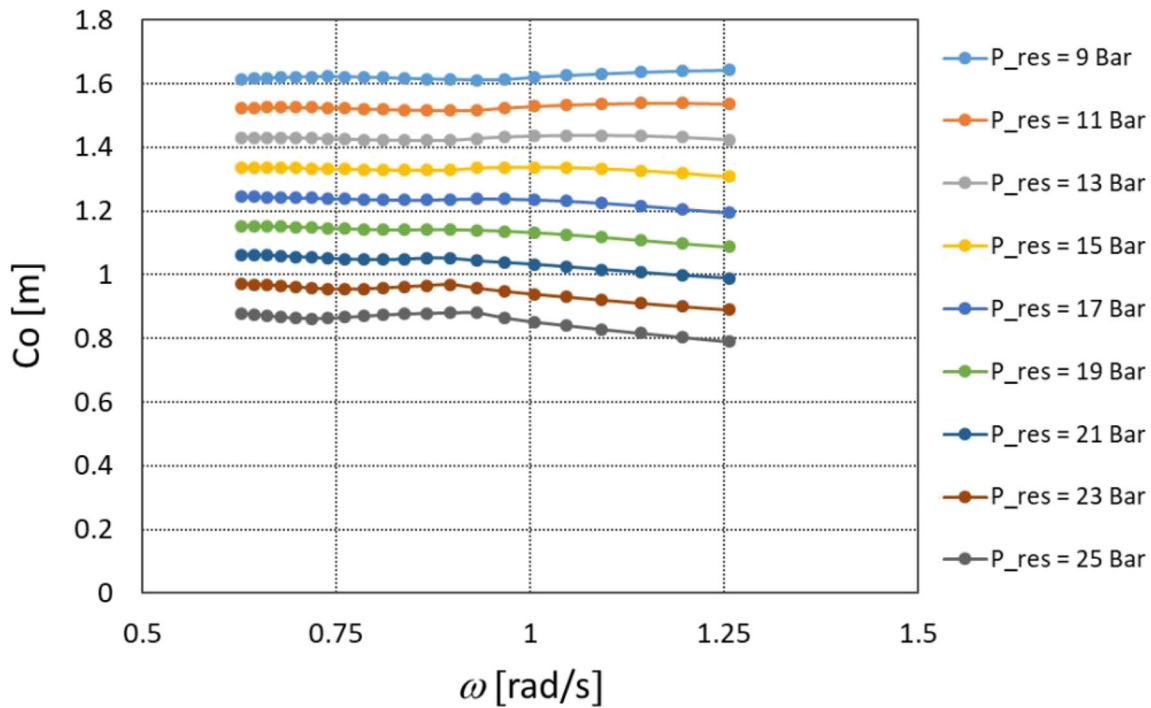


FIGURE 20 Trend of the piston stroke C_o by changing the circular frequency and the pressure of the reservoir, for a wave of 2 m height [Colour figure can be viewed at wileyonlinelibrary.com]

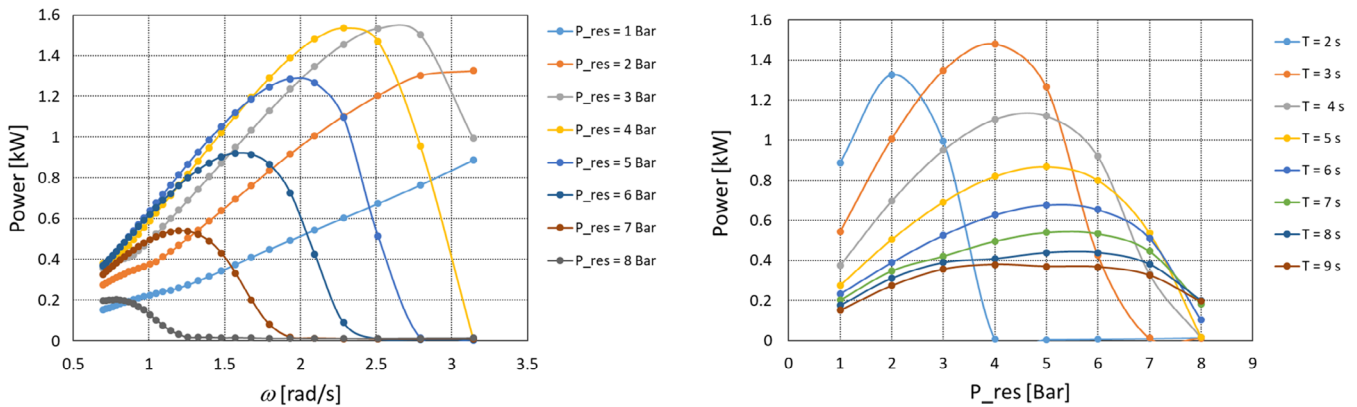


FIGURE 21 Trend of the system power by changing the circular frequency and the pressure of the reservoir, for a wave of 0.4 m height [Colour figure can be viewed at wileyonlinelibrary.com]

of the reservoir, p_{res} . This analysis was repeated for wave height changing from 0.4 m (Figure 16) to 2 m (Figure 20) with step of 0.4 m.

The previous figures show that the trend of the stroke of the piston pump is quite flat for low circular frequency (high period of the wave) and for height of the waves higher than 0.8 m. It diminishes with the higher pressures of the reservoir. The pressure of the reservoir influences also the sinking z_A of the buoy, as illustrated in Equations (23) and (24).

5.3 | Power of the system

Next graphs, from Figures 21 to 25, illustrate the variations of the system power for different wave heights ($H_w = 0.4$ m, 0.8 m, 1.2 m, 1.6 m, 2 m) by changing the circular frequency $\omega = 2\pi/T$ and the pressure of the reservoir $p_{res} = \rho g H_m$. Each figure is composed by two graphs, which show the same power variation: the left graph shows the power curves vs the circular frequency ω for different pressure levels, the right graph shows the

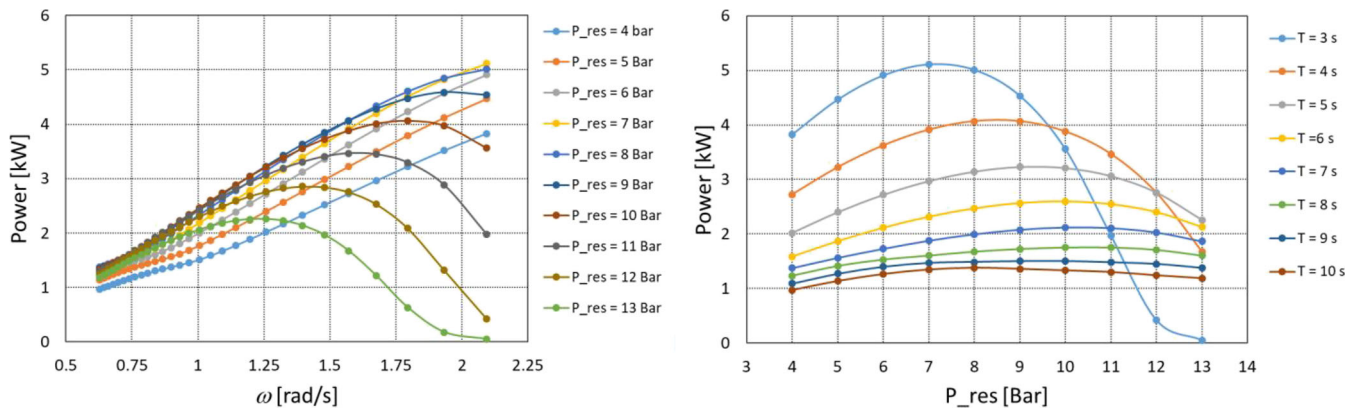


FIGURE 22 Trend of system power by changing the circular frequency and the pressure of the reservoir, for a wave of 0.8 m height [Colour figure can be viewed at wileyonlinelibrary.com]

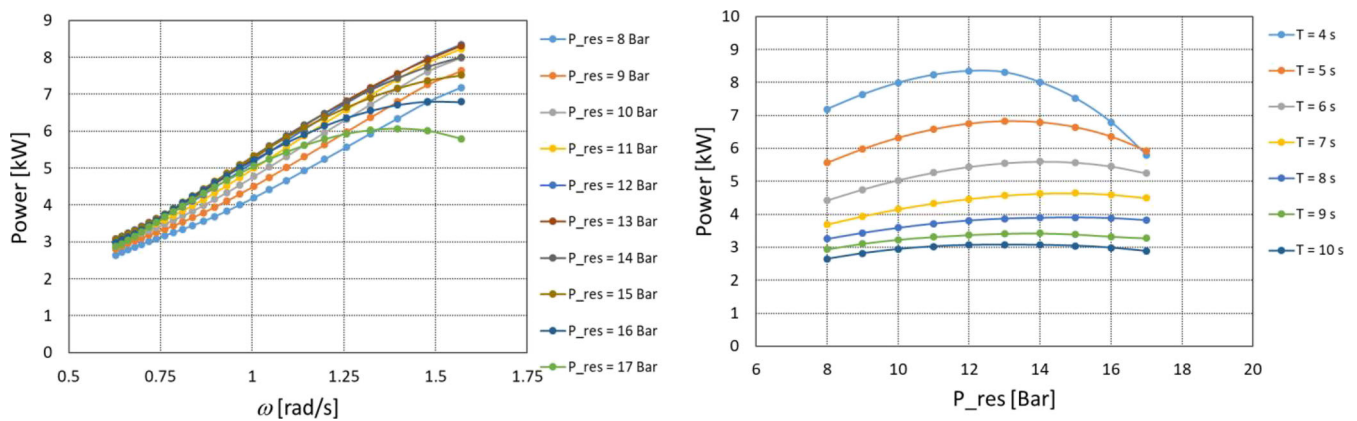


FIGURE 23 Trend of the system power by changing the circular frequency and the pressure of the reservoir, for a wave of 1.2 m height [Colour figure can be viewed at wileyonlinelibrary.com]

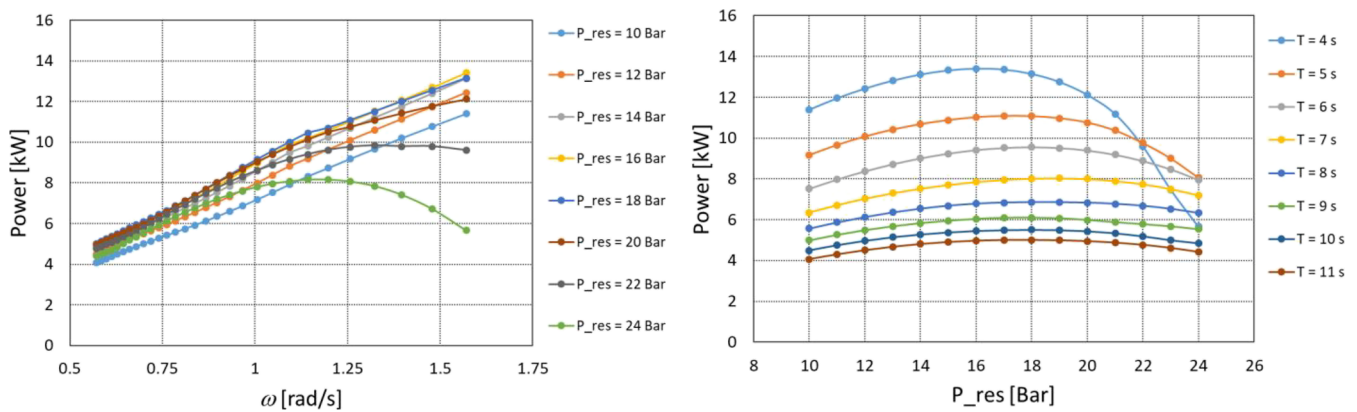


FIGURE 24 Trend of the system power by changing the circular frequency and the pressure of the reservoir, for a wave of 1.6 m height [Colour figure can be viewed at wileyonlinelibrary.com]

power curves vs the pressure of the reservoir, for different periods $T = 2\pi/\omega$ of the wave.

From the previous figures, it is clear that the lower the circular frequency (long wave period), the smaller the

power of the system. At this point, it is necessary to observe that not all frequencies have the same importance. Those that occur most often are more relevant for the purpose of acquiring energy.

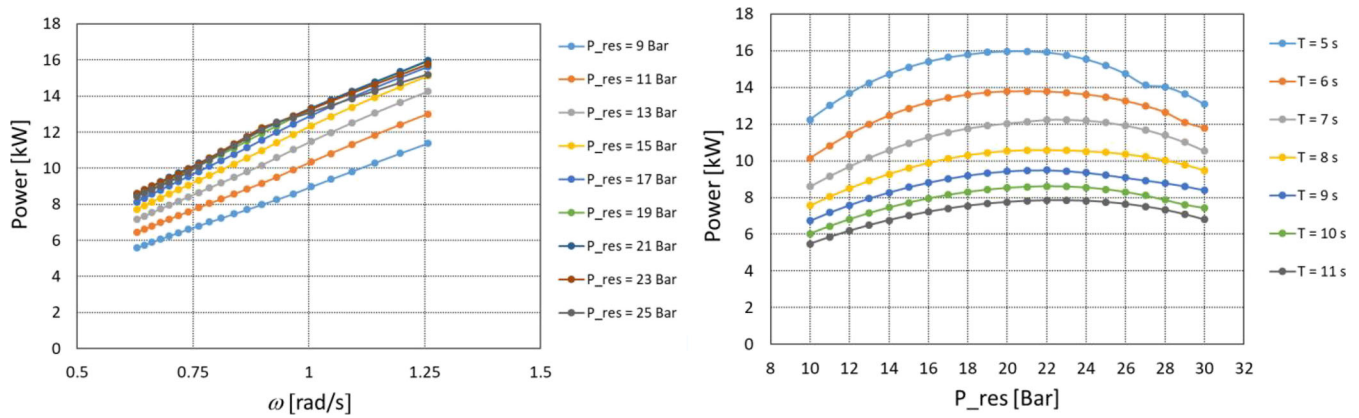


FIGURE 25 Trend of the system power by changing the circular frequency and the pressure of the reservoir, for a wave of 2 m height [Colour figure can be viewed at wileyonlinelibrary.com]

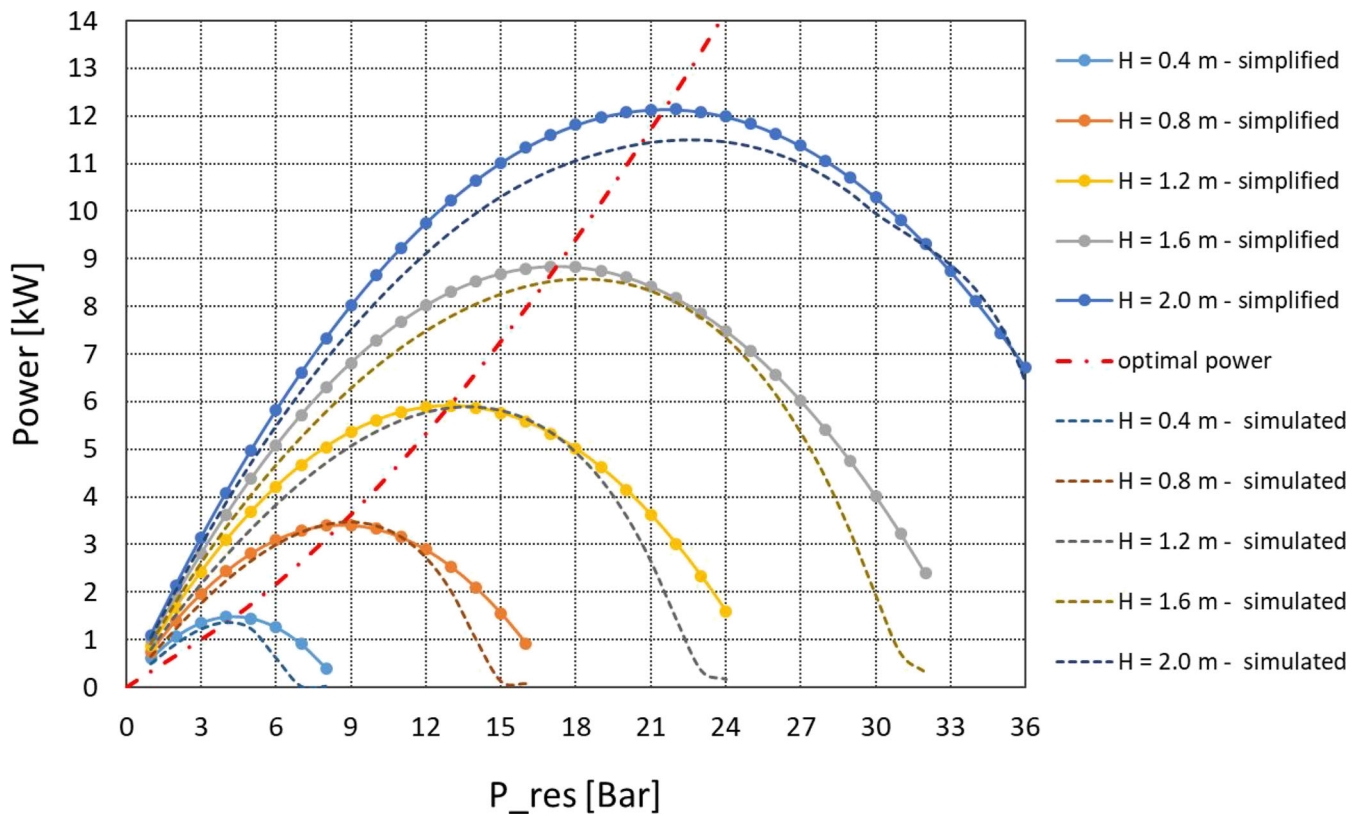


FIGURE 26 Trend of the power obtained with the Matlab-Simulink @ code (dashed lines) compared with the simplified formulas of Equations (52) and (53) [Colour figure can be viewed at wileyonlinelibrary.com]

Anyway, for each circular frequency or T-wave period, the optimal reservoir pressure guarantees the maximum power.

The next figure, Figure 26, reports the powers related to different wave height (from 0.4 to 2 m) by changing the pressure of the reservoir both obtained with the simplified Equation (52) and by the Simulink code (dashed lines) and the optimal power line (red dashed line) which connects the maximum values.

The curves of power obtained with the simplified formula of Equation (52) have the same trend of those obtained from the simulations even if the values are slightly higher (maximum error of about 10%). Anyway, the maximum values are approximately obtained for the same value of pressure of the reservoir. These results are very important because they confirm the validity of Equation (54), that is, the optimal pressure of the reservoir has a linear trend with the height of the wave.²⁷

TABLE 4 Number of events associate with the waves accounted by the buoy RON

height→ period↓	From 0.0 to 0.2	From 0.2 to 0.4	From 0.4 to 0.6	From 0.6 to 0.8	From 0.8 to 1.0	From 1.0 to 1.2	From 1.2 to 1.4	From 1.4 to 1.6	From 1.6 to 1.8	From 1.8 to 2.0	From 2.0 to 2.2	From 2.2 to 2.4	From 2.4 to 2.6	From 2.6 to 2.8	From 2.8 to 3.0	From 3.0 to 3.2	From 3.2 to 3.4	From 3.4 to 3.6	From 3.6 to 3.8	From 3.8 to 4.0
from 0 to 0.25	0	0	0	0	0	0	0	0	0	0	0	0	0	0	0	0	0	0	0	0
from 0.25 to 0.5	0	0	0	0	0	0	0	0	0	0	0	0	0	0	0	0	0	0	0	0
from 0.5 to 0.75	0	0	0	0	0	0	0	0	0	0	0	0	0	0	0	0	0	0	0	0
from 0.75 to 1	0	0	0	0	0	0	0	0	0	0	0	0	0	0	0	0	0	0	0	0
from 1 to 1.25	0	0	0	0	0	0	0	0	0	0	0	0	0	0	0	0	0	0	0	0
from 1.25 to 1.5	0	0	0	0	0	0	0	0	0	0	0	0	0	0	0	0	0	0	0	0
from 1.5 to 1.75	0	0	0	0	0	0	0	0	0	0	0	0	0	0	0	0	0	0	0	0
from 1.75 to 2	85	7	0	0	0	0	0	0	0	0	0	0	0	0	0	0	0	0	0	0
from 2 to 2.25	563	65	0	0	0	0	0	0	0	0	0	0	0	0	0	0	0	0	0	0
from 2.25 to 2.5	1403	92	3	0	0	0	0	0	0	0	0	0	0	0	0	0	0	0	0	0
from 2.5 to 2.75	1272	177	11	0	0	0	0	0	0	0	0	0	0	0	0	0	0	0	0	0
from 2.75 to 3	1172	299	24	0	0	0	0	0	0	0	0	0	0	0	0	0	0	0	0	0
from 3 to 3.25	875	528	29	1	0	0	0	0	0	0	0	0	0	0	0	0	0	0	0	0
from 3.25 to 3.5	582	760	63	9	0	0	0	0	0	0	0	0	0	0	0	0	0	0	0	0
from 3.5 to 3.75	398	945	91	12	2	0	0	0	0	0	0	0	0	0	0	0	0	0	0	0
from 3.75 to 4	225	954	171	29	4	0	0	0	0	0	0	0	0	0	0	0	0	0	0	0
from 4 to 4.25	154	836	241	76	9	0	0	0	0	0	0	0	0	0	0	0	0	0	0	0
from 4.25 to 4.5	130	817	356	94	18	3	9	1	0	0	0	0	0	0	0	0	0	0	0	0
from 4.5 to 4.75	70	754	503	149	42	7	3	0	0	0	0	0	0	0	0	0	0	0	0	0
from 4.75 to 5	50	484	629	212	68	29	4	1	0	0	0	0	0	0	0	0	0	0	0	0
from 5 to 5.25	26	360	663	272	119	42	19	3	0	1	0	0	0	0	0	0	0	0	0	0
from 5.25 to 5.5	23	258	569	362	170	70	25	10	4	0	2	0	0	0	0	0	0	0	0	0
from 5.5 to 5.75	16	170	379	405	170	84	38	12	8	1	2	0	0	0	0	0	0	0	0	0
from 5.75 to 6	7	112	288	392	186	128	60	20	11	5	2	0	0	0	0	0	0	0	0	0
from 6 to 6.25	4	84	178	360	280	154	81	40	20	10	5	2	0	0	0	0	0	0	0	0
from 6.25 to 6.5	6	51	102	211	271	183	115	71	29	4	6	5	6	1	0	0	0	0	0	0
from 6.5 to 6.75	2	46	60	117	204	176	150	85	45	23	13	4	3	2	1	0	0	0	0	0
from 6.75 to 7	0	26	49	77	115	171	143	93	56	47	16	8	6	0	0	0	0	0	0	0
from 7 to 7.25	2	13	30	58	74	100	125	95	77	49	20	14	11	5	3	0	0	0	0	0
from 7.25 to 7.5	0	9	22	30	52	60	76	84	57	50	36	24	10	8	6	3	1	0	0	0

(Continues)

TABLE 4 (Continued)

height→ period↓	From 0.0 to 0.2	From 0.2 to 0.4	From 0.4 to 0.6	From 0.6 to 0.8	From 0.8 to 1.0	From 1.0 to 1.2	From 1.2 to 1.4	From 1.4 to 1.6	From 1.6 to 1.8	From 1.8 to 2.0	From 2.0 to 2.2	From 2.2 to 2.4	From 2.4 to 2.6	From 2.6 to 2.8	From 2.8 to 3.0	From 3.0 to 3.2	From 3.2 to 3.4	From 3.4 to 3.6	From 3.6 to 3.8	from 3.8 to 4.0
from 7.5 to 7.75	0	10	18	15	23	45	49	67	60	33	49	24	17	9	9	6	4	0	0	0
from 7.75 to 8	0	4	10	16	15	19	32	47	43	40	41	24	13	16	11	6	1	4	3	0
from 8 to 8.25	0	2	9	13	10	16	17	32	40	29	19	24	18	18	12	8	5	6	4	1
from 8.25 to 8.5	0	4	6	7	3	7	7	18	21	18	16	17	18	12	12	11	3	5	3	3
from 8.5 to 8.75	0	0	4	7	9	8	5	8	17	8	13	19	11	9	11	10	5	6	5	4
from 8.75 to 9	0	0	0	7	6	4	2	8	8	9	5	7	6	12	4	9	8	8	3	9
from 9 to 9.25	0	0	2	5	5	2	3	2	3	8	8	2	4	4	2	2	2	3	9	2
from 9.25 to 9.5	0	0	0	0	4	4	3	3	0	4	3	3	2	4	3	3	6	3	5	2
from 9.5 to 9.75	0	0	0	2	4	3	1	3	2	2	1	5	5	2	5	3	4	3	1	2
from 9.75 to 10	0	0	0	0	2	0	0	2	1	2	1	2	0	22	0	6	3	0	0	0
from 10 to 10.25	0	0	0	0	1	0	0	2	0	0	1	1	1	1	1	0	0	3	3	1
from 10.25 to 10.5	0	0	0	0	1	0	1	0	1	0	0	0	1	0	0	1	3	0	0	1
from 10.5 to 10.75	0	0	0	0	0	0	0	0	1	1	0	0	0	0	0	0	2	0	0	2
from 10.75 to 11	0	0	0	0	0	0	0	0	0	0	0	0	0	0	0	0	0	0	0	1
from 11 to 11.25	0	0	0	0	0	0	0	0	0	0	0	1	0	0	0	0	0	0	0	0
from 11.25 to 11.5	0	0	0	0	0	0	0	0	0	0	0	0	1	0	0	0	0	0	0	0
from 11.5 to 11.75	0	0	0	0	0	0	0	0	0	1	0	0	0	0	0	0	0	0	0	0
from 11.75 to 12	0	0	0	0	0	0	0	0	0	0	0	0	0	0	0	0	0	0	0	0
from 12 to 12.25	0	0	0	0	0	0	0	0	0	0	0	0	0	0	0	0	0	0	0	0
SUM	7065	7867	4510	2938	1867	1315	968	707	504	345	259	186	133	105	82	62	56	44	38	28
FREQUENCIES	24.30%	27.05%	15.51%	10.10%	6.42%	4.52%	3.33%	2.43%	1.73%	1.19%	0.89%	0.64%	0.46%	0.36%	0.28%	0.21%	0.19%	0.15%	0.13%	0.10%

In the specific case, having a buoy with an area of 12 m², the optimal pressure expressed in bar is

$$(p_{res})_{opt} = 11H_w \tag{61}$$

5.4 | Energy output of the Cetraro site

The site of Cetraro has been introduced in the previous section. Here a more detailed table, Table 4, reports for each wave, characterized by a certain height and period, the number of events averaged on 8 years. The total number of events is 29 079, which implies about 3 measurements per hour. The green cells contain, for each height of the waves, the periods more frequent or peak periods. The trend follows more or less that proposed in Reference 12.

Anyway, by means of the proposed model, it has been possible to calculate for each cell of Table 4 the power of the system. Therefore, by considering the number of events of the cell itself, the yearly energy is obtained by multiplying the power by the number of events and dividing by 3.

Figure 27 illustrates the energy of each wave height: the maximum energy output is about 2000 kWh provided by the wave of 0.7 m height (about the design value). The total energy output is evaluated around 22 464.4 kWh/year. This result, given by a buoy having 12 m² area, is encouraging since the site of Cetraro have not a great potential energy.

Finally, the total capture width ratio has been evaluated by considering the total amount of energy respect to the ideal energy, as it follows:

$$CWR = 100 \frac{E_{out}}{D_{buoy} \sum J_{Hw} n_e} = 25\% \tag{62}$$

The proposed technology does not require particular interventions for shaping the seabed since it has a fixed part on-shore and is developed in calm seas characterized by low energy potential. For this reason, it is easy to apply and cheap enough.²⁸

Moreover, differently from other technologies, like Pelamis²⁴ or Archimedes waveswing (oscillating system),²⁵ the proposed system is very easy to install, since the workers have the possibility of laying their machinery on shore.

The possibility of being integrated into breakwaters makes the proposed solution even cheaper, since the seabed shaping costs are attributed to environmental protection.

To complete the present analysis, Table 5 reports a rough costs estimation split into various items.

TABLE 5 Costs estimation

Basement and seabed modeling	€ 30 000
Pump and buoy	€ 10 000
Piping	€ 5000
Reservoir and tank	€ 3000
Micro Pelton turbine	€ 15 000
Power house	€ 7000
Total	€ 70 000

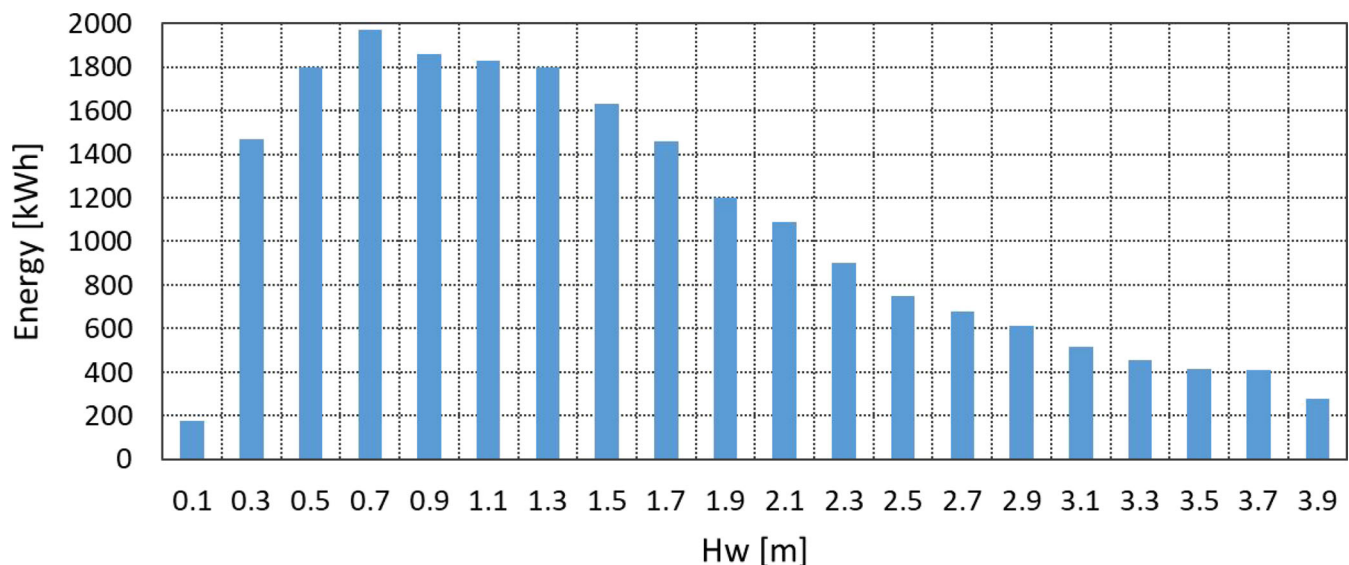


FIGURE 27 Yearly energy of each wave height of the Cetraro site [Colour figure can be viewed at wileyonlinelibrary.com]

The costs of the investment, by considering state incentives of 0.34 €/kWh, could be recovered in little more than 9 years.

6 | CONCLUSIONS

In this paper, a new system exploiting energy from waves near the shore is proposed, composed by an oscillating buoy, which incorporates a piston pump, able to deliver water to a pressurized tank feeding a micro Pelton turbine.

The first part of the paper provides an extensive mathematical approach, useful to simulate the motion of the oscillating buoy (point absorber), which allows to compute the power of the system in various conditions related to waves having different heights and periods.

The mathematical model permitted to derive some simplified formulas, valuable for defining a sizing procedure for designing all the components of the system. That is an important finding useful to enable designers to estimate quickly the feasibility of the plant, starting from the energy resource of the site.

Depending on the waves distribution, the system can be scaled to small powers so being able to work in sites characterized by waves with low potential energy. In islands, it could resolve problems related to energy supply and storage, being easily to integrate with other energy sources in mini- or micro-grids.

A first design has been done for the Calabrian site of Cetraro where a mean energy flux of 2.7 kW/m²/year is estimated. By applying the proposed sizing procedure, the main identified components that is, the buoy, the piston pump, the piping, the pressurized reservoir and the Pelton turbine, were designed. Their dimensions are quite small, given the height of the design wave of 0.8 m, below which more than 77% of the waves occur in this site.

The system has been designed for working always in optimal conditions: in fact, for each waves there is an optimal value of the pressure of the reservoir, which guarantees the maximum power.

The pressure of the reservoir has then to be changed according to the height of the wave. For doing that, the flow rate of the Pelton turbine is changed by opening or closing the nozzle area.

However, at peak periods of the waves (most frequent periods), an optimal opening of the nozzle area can guarantee this optimal working, being the incoming flow rates of the piston pump, able to change the pressure of the reservoir in the right way.

Waves from 0.1 m until 4 m are easily managed by changing the pressure of the reservoir from 1 up to 40 bar. So doing, the power of the system changes from 3 to 36 kW.

Therefore, with the use of a buoy capture surface of 12 m², it results that about 22 464 kWh/year could be produced on the Cetraro site, so exploiting 25% (CWR) of the overall energy source. The costs of the system were estimated around € 70 000, with a payback period of about 9 years.

Future works will regard an experimental phase, since the authors are involved in setting up a small buoy prototype for testing it in a laboratory channel flow. The experiments, done in different operating conditions even by using diverse buoy shapes, will further validate the model results.

ACKNOWLEDGEMENTS

An important contribution to the success of this work came from the availability of data on marine waves detected by the Italian National Buoy Network (RON). The authors wish to thanks the ENEA Researchers G. Sannino and A. Carillo, who kindly have provided this information, recorded over a long period (8 years) in the buoy of Cetraro (Italy).

NOMENCLATURE

A_{buoy}	buoyant area (m ²)
A_n	turbine nozzle area (m ²)
A_p	piston area (m ²)
A_{pipe}	pipe area (m ²)
b	viscous damping coefficient (kg/s)
B	buoy width (m)
C_D	drag coefficient (-)
C_o	pump stroke (m)
c_o	spouting velocity (m/s)
CWR	capture width ratio (%)
D	buoy draft (m)
D_B	cylindrical buoy diameter (m)
D_{buoy}	characteristic size of the buoy (m)
D_n	nozzle diameter (m)
D_p	piston diameter (m)
D_{pipe}	pipe diameter (m)
D_T	turbine diameter (m)
f	pipe friction coefficient (-)
f_{cy}	wave frequency (Hz)
F_A	Archimedes' force (N)
F_{ex}	exciting force (N)
$F_{ex,a}$	amplitude of the exciting force (N)
F_W	weight force (N)
F_p	pressure force (N)
F_{PTO}	power take off force (N)
g	gravity (m/s ²)
h	seabed depth (m)
H_{buoy}	buoy height
H_m	reservoir pressure expressed in water column meters (m)

H_w	wave height (m)
$H_s, H_{1/3}$	significant wave height (m)
J	average wave power (kW/m)
k	specific turbine speed (–)
k	wave number (m^{-1})
L	buoy length (m)
L_{max}	absorption width (m)
L_{pipe}	pipes length (m)
m_{add}	added mass (kg)
m_b	buoyant mass (kg)
N_{cy}	wave frequency (min^{-1})
n_e	number of events (–)
n_T	turbine rotational speed (rpm)
p_{res}	pressure of the reservoir (bar)
P_{av}	average power (kW)
P_P	pump power (kW)
P_{System}	system power (kW)
P_T	turbine power (kW)
Q_P	pump flow rate (m^3/s)
Q_T	turbine flow rate (m^3/s)
S_w	wetted surface (m^2)
T_e	wave period (s)
u	peripheral velocity (m/s)
V_{air}	air volume (m^3)
V_P	pump volume (m^3)
V_{res}	reservoir volume (m^3)
z	vertical position of the buoy (m)
z_A	sinking of the buoy due to the pressure (m)
z_w	sinking of the buoy due to the weight (m)

GREEK LETTERS

β	deflection turbine blade angle ($^\circ$)
γ	damping ratio (–)
φ	phase displacement ($^\circ$)
φ_v	velocity reduction coefficient (–)
η_{el}	electrical efficiency (–)
η_P	hydraulic piping efficiency (–)
η_T	turbine efficiency (–)
λ	wave length (m)
ρ	water density (kg/m^3)
ψ	velocity reduction coefficient (–)
ω_o	peak or natural circular frequency (rad/s)
ω	circular frequency (rad/s)

ORCID

Silvio Barbarelli  <https://orcid.org/0000-0002-8670-9955>

Teresa Castiglione  <https://orcid.org/0000-0001-8882-8037>

REFERENCES

- Nastasi B, Lo Basso G, Astiaso Garcia D, Cumo F, de Santoli L. Power-to-gas leverage effect on power-to-heat application for urban renewable thermal energy systems. *Int J Hydrogen Energ.* 2018;43(52):23076-23090, ISSN 0360-3199. <https://doi.org/10.1016/j.ijhydene.2018.08.119>.
- Raju Ahamed, Kristoffer McKee, Ian Howard. Advancements of wave energy converters based on power take off (PTO) systems: a review. *Ocean Eng* Volume 204, 2020, 107248. Available from: <https://doi.org/10.1016/j.oceaneng.2020.107248>
- Wang Z, Carriveau R, Ting DS-K, Xiong W, Wang Z. A review of marine renewable energy storage. *Int J Energ Res.* 2019;43: 6108-6150. <https://doi.org/10.1002/er.4444>.
- Liu Z, Qu N, da Shi H. Experimental study on hydrodynamic performance of a wave energy converter within multi-heaving-buoys. *Int J Energ Res.* 2017;41:1351-1366. <https://doi.org/10.1002/er.3725>.
- S. S. Prakash, K. A. Mamun, F.R. Islam, R. Mudliar, C. Pau'u, M. Kolivuso, S. Cadrilala. Wave energy converter: a review of wave energy conversion technology. 2016 3rd Asia-Pacific World Congress on Computer Science and Engineering, 2017, Article number 7941943: 71–77. <https://doi.org/10.1109/APWC-on-CSE.2016.023>
- Zhang H, Zhou B, Vogel C, Willden R, Zang J, Zhang L. Hydrodynamic performance of a floating breakwater as an oscillating-buoy type wave energy converter. *Appl Energy.* 2020;257:113996. <https://doi.org/10.1016/j.apenergy.2019.113996>.
- Hu J, Zhou B, Vogel C, et al. Optimal design and performance analysis of a hybrid system combing a floating wind platform and wave energy converters. *Appl Energy.* 2020;269:114998. Available from: <https://doi.org/10.1016/j.apenergy.2020.114998>.
- IEA. Brito-Melo A., Hukerby J., *Implementing Agreement on Ocean Energy Systems*. Portugal: Executive Committed of the OES-IA; 2010. <https://ita.calameo.com/read/000672419bcd39df865dc>
- Markos I. Bonovas, Ioannis S. Anagnostopoulos. Modelling of operation and optimum design of a wave power take-off system with energy storage. *Renew Energy* Volume 147, Part 1, 2020, Pages 502–514. <https://doi.org/10.1016/j.renene.2019.08.101>
- Silvio Barbarelli, Gaetano Florio, Giacomo Lo Zupone, Nino Michele Scornaienchi. First techno-economic evaluation of array configuration of self-balancing tidal kinetic turbines. *Renew Energy*, December (2018), Volume 129A, Part A, Pages 183–200, doi: <https://doi.org/10.1016/j.renene.2018.06.007>
- Piotr Zwolan, Krzysztof Czaplowski. Sea waves models used in maritime simulators. *Sci J, Maritime University of Szczecin*, 2012, 32(104) z. 2 pp. 186–190.
- Pierson WJ Jr, Moskowitz LA. Proposed spectral form for fully developed wind seas based on the similarity theory of S. A. Kitaigorodskii. *J Geophys Res.* 1964;69:5181-5190.
- Cook J. Investigating the concept of a novel flexible fabric wave energy device. *Plymouth Student Sci.* 2015;8(1):167-185. <http://hdl.handle.net/10026.1/14090>.
- Garcia-Rosa PB, Cunha JPVS, Lizarralde F. *Turbine Speed Control for an Ocean Wave Energy Conversion System*. St. Louis, MO: American Control Conference Hyatt Regency Riverfront; 2009:10-12.
- Tampier G, Grueter L. Hydrodynamic analysis of a heaving wave energy converter. *Int J Mar Energy.* 2017;19:304-318. <https://doi.org/10.1016/j.ijjome.2017.08.007>.
- Barbarelli S, Florio G, Amelio M, Scornaienchi NM. Preliminary performance assessment of a novel on-shore system recovering energy from tidal currents. *Appl Energy.* 2018;224: 717-730. <https://doi.org/10.1016/j.apenergy.2018.05.029>.

17. Faltinsen OM. *Hydrodynamics of High-Speed Marine Vehicles*. New York, NY: Cambridge University Press; 2005.
18. Kool W, Kim J-D. Simplified formulas of heave added mass coefficients at high frequency for various two-dimensional bodies in a finite water depth. *Int J Nav Archit Ocean Eng*. 2015;7: 115-127. <https://doi.org/10.1515/ijnaoe-2015-0009>.
19. Sannino G, Bargagli A, Carillo A, Caiaffa E, Lombardi E, Monti P, Leuzzi G. Valutazione del potenziale energetico del moto ondoso lungo le coste italiane. *ENEA, Report RdS/2011/151*. 4-32.
20. Falnes J. Ocean waves and oscillating systems: linear interactions including wave-energy extraction. *Appl Mech Rev*. 2003; 56:B3. <https://doi.org/10.1115/1.1523355>.
21. Shadman M, Estefen SF, Rodriguez CA, Nogueira ICM. A geometrical optimization method applied to a heaving point absorber wave energy converter. *Renew Energy*. 2018;115:533-546. <https://doi.org/10.1016/j.renene.2017.08.055>.
22. Twidell J, Weir T. *Renewable Energy Resources*. 3rd ed. London: Taylor & Francis Group. Imprint: Routledge; 2015.
23. Falnes J, Lillebekken PM. Budal's latching-controlled-buoy type wave-power plant. *Proceedings of the Fifth European Wave and Energy Conference*; Hydraulics & Maritime Research Centre. 2003:233-244. <http://hdl.handle.net/11250/246687>.
24. Pelamis Wave Power. <http://www.emec.org.uk/about-us/wave-clients/pelamis-wave-power/>
25. Archimedes waveswing submerged wave power buoy. <http://www.awsocan.com/archimedes-waveswing.html>
26. Liberti L, Carillo A, Sannino G. Wave energy resource assessment in the Mediterranean, the Italian perspective. *Renew Energy*. 2013;50:938-949.
27. Barbarelli S, Amelio M, Florio G, Scornaienchi NM. Study of a hydraulic system converting energy from sea waves near the coast. *MATEC Web Conf*. 2018;240:1-6. <https://doi.org/10.1051/mateconf/201824001004>.
28. Barbarelli S, Amelio M, Castiglione T, Florio G. Nino Michele Scornaienchi hydraulic on-shore system recovering energy from sea waves. *Energy Proc*. 2019;159:72-77. <https://doi.org/10.1016/j.egypro.2018.12.021>.
29. Rico H, Hansen, Morten M, Kramer and Enrique Vidal. Discrete displacement hydraulic power take-off system for the Wavestar wave energy converter. *Energies* 2013, 6, 4001-4044; available from: <https://doi.org/10.3390/en6084001>

How to cite this article: Barbarelli S, Amelio M, Castiglione T, Florio G, Scornaienchi NM. Design and analysis of a new wave energy converter based on a point absorber and a hydraulic system harvesting energy from waves near the shore in calm seas. *Int J Energy Res*. 2020;1-30. <https://doi.org/10.1002/er.5799>